EVOLUTIVE FRACTURE BEHAVIOR OF CEMENTED PASTE BACKFILL

by

Sami Hasan

A thesis
submitted to the Faculty of Graduate Studies
in partial fulfilment of the requirements for the
Degree of Master of Science
in

Civil Engineering

Supervisor
Dr. Liang Cui
Associate Professor – Dept. of Civil Engineering

Lakehead University
Thunder Bay, Ontario
August 2022

Author's Declaration Page

I hereby declare that I am the sole author of this thesis. This is a true copy of the thesis, including any required final revisions, as accepted by my examiners. I understand that my thesis may be made electronically available to the public.

Abstract

Underground mining is a key global industry that produces many of the mineral resources needed by several sectors of the economy. However, underground mining extracts large volumes of material from below the ground, which not only creates substantial subsurface voids, bult also produces high volumes of solid waste. Consequently, the potentially catastrophic failure of underground openings and environmental issues such as acid mine drainage has attracted increasing attention. To ensure the safety of mining workers and equipment and sustainably reuse the mine waste materials, cemented paste backfill (CPB, an engineered mixture of tailings, hydraulic binder, and water) technology has been widely adopted in underground mines around the world. Since CPB materials are used as the key ground support measure, the mechanical behaviors and properties play crucial roles in the safe design of CPB under complex field loading conditions. As a type of cementitious materials, the failure process is governed by the development of tensile and shear crack in CPB matrix under various loading conditions. Meanwhile, due to the progression of cement hydration, CPB materials also demonstrate curing time-dependent evolution of mechanical behaviors and properties. Moreover, a considerable amount of water is utilized to prepare the CPB paste and thus affects the particle interaction and cement hydration. Therefore, it is of theoretical and practical importance to investigate the effect of mix recipe and hydraulic factors on the evolutive fracture behavior and properties of CPB under mode-I (i.e., tensile stress), mode-II (in-plane shear stress), and mode-III (out-of-plane shear stress) loading conditions at different curing times. However, previous studies focus mainly on the conventional geomechanical behaviors, including compressive, tensile, and shear behaviors, of CPB. No studies have been designed and conducted to systematically investigate the effect of mix recipe and hydraulic factors on the evolutive fracture behavior and properties of CPB materials. To address such a research gap, a comprehensive experimental testing program consisting of semi-circular bend (SCB) tests, end notched disc bend (ENDB) tests, measurements of gravimetric water content (GWC), and scanning electron microscopy (SEM) analysis are developed and successfully implemented through this thesis research. Moreover, for the effect of cement content, three different cement contents, including 2wt%, 4.5wt%, and 7wt%, are adopted to prepare CPB samples that are cured at 7, 28, and 90 days. For the effect of hydraulic factors, three factors, including water-to-tailings ratios (0.33, 0.36, and 0.39), drained and undrained conditions, and resaturation conditions, are

considered in this study. The obtained results show that the changes in cement content affect the pre- and post-peak fracture behaviors of CPB. Moreover, it has been identified that the fracture toughness is highly sensitive to the cement content for the effect of hydraulic factors. It has been found that water content plays a critical role in the early-age fracture behavior and properties. However, after 28 days, the improvement of fracture properties associated with water drainage conditions and resaturation conditions is limited. In addition, it has also been found that the tensile fracture toughness is higher than the shear (both mode-II and mode-III) fracture toughness of CPB from early to advanced ages. The obtained findings have the potential to improve the undergrounding of the effect of chemical and hydraulic factors on the evolutive fracture behavior of CPB materials and thus contribute to the safe implementation of CPB technology in underground mines.

Acknowledgements

Firstly, I would like to thank my Supervisor, Dr. Cui, for his advice and guidance in writing this thesis.

A big thanks to my parents, Ahmad and Maha, for always being there for me. Without their support, I would not be here today.

Thanks to my fellow team members Aaron, Brett, and Javaughn, for their help in and out of the lab. I enjoyed our time working together. I would also like to extend thanks to the lab staff, Cory and Morgan, for providing their time and assistance in the lab whenever needed.

To my thesis examiners, Dr. Kun Fang and Dr. Wa Gao, thank you for taking your time and consideration of my work. The suggestions and insight provided by you both were extremely valuable and greatly improved the quality of my research.

Contents

List of Figures

List of Tables

Nomenclature

Cc	Cement Content
CPB	Cement Paste Backfill/ Cemented Paste Backfill
DoS	Degree of Saturation. Can be described as fully saturated (100%), unsaturated (0%), or partially saturated (100%>x>0%).
Work	The amount of energy put into the material. The work of crack initiation represent the energy used to begin forming a crack in the sample.
N	Newton, unit of force.
A	area of the mould cross section, which is circular. $A = \pi r^2 H$ [cm^2]
H	height of the mould [cm]
V	total volume of the mould [cm^3]
Y_{CPB}	Density of CPB
M	mass of CPB in the sample mold [kg]
Cc	percent of cement content in the mix by weight
M_c	mass of cement [kg]
M_T	mass of tailings [kg]
M_w	mass of water [kg]
K_n	Fracture toughness for Mode-n
P	Peak [N]
D	diameter of semicircular specimen (m)
T	thickness of semicircular specimen (m)
a	notch length (m)
B	thickness of the disc specimen
S	horizontal distance between central and edge bars
R	radius of the disc specimen

β	inclination of notch line w.r.t. the central bar
Y_n	normalized stress intensity factor for Mode-n (dimensionless)
SCB	Semi-Circular Bend test
ENDB	End-Notch Disk Bend test

Chapter 1 Introduction

1.1 Background

Mining is a key global industry that produces many of the resources needed by several sectors of the economy. Underground mining removes large volumes of material from the ground, creating potentially unsafe areas above and below ground while producing high volumes of waste. In order to prevent the collapse of mining tunnels and stopes, the cut and fill method adds fill material in the mined areas to ensure structural integrity. Traditionally, backfill techniques can consist of several materials. In cemented rock fill, rock material is mixed with cement binder to act as support. This system uses low cement content to bind the rocks.

The mining waste comes in the form of mine tailings, which are often collected in tailing ponds for ease of storage. There is also a risk of mine collapse as operations continue due to the removal of supporting rock. To ensure safety during and after mining, the voids in mines must be filled throughout the operation. Cement Paste Backfill (CPB) has seen a rising use in recent years as a way to support walls during mining operations. (Xu et al, 2019; Fang and Fall, 2018; Pan and Grabinsky, 2021). CPB consists of dewatered mine tailings, which is waste material from mining mixed with cement and water (Qi and Fourie, 2019; Liu et al, 2019; Tian and Fall, 2021). Several advantages to the use of CPB include the reduction and reuse of mining waste (Cheng et al, 2021; Liu et al, 2019), removal of dangerous tailing ponds (Wang et al, 2021), and inexpensive backfill material, easy to prepare in-situ. The fracture toughness is used to measure the strength of a material when it has a pre-existing defect. This measure is highly applicable to CPB due to the nature of its application. CPB is often poured against the wall of a mine, which is a rock with unsmooth and random geometries. In this case, some cross-sections of the CPB stope will be thin relative to the rest of the stope. It is at these points that a pre-existing defect is naturally introduced into the material. These points are the most likely to fail, so the need for understanding the behavior of these materials is clear. In fracture mechanics, three fracture modes are recognized, known as mode, I, II, and III. Each mode corresponds to a different crack propagation. Weak planes can also occur at the interface of two different materials (Huang et al, 2020). This can include the internal interfaces of early CPB, interface between different CPB stopes, and rock interface. Mode-I

represents tension failure, where the pre-existing failure expands out due to applied stress. This can occur, as seen in Figure 1.1-A. Mode-II represents in-plane shear stress (1.1-B), and Mode-III represents out-of-plane shear stress, as seen in Figure 1.1-C (Roylance, 2001). Pure Mode-III occurs when the defect is offset from the plane of the load by an angle over 62 degrees (Aliha and Bahmani, 2017). Meanwhile, an angle of less results in a mixed-mode failure.

Engineering design of CPB is commonly through a material strength-based design approach. Specifically, this design method can be represented as the factor of safety, FS, which can be calculated as the strength divided by the stress. Theoretically speaking, FS equal to one means that the prepared CPB meets the design requirements on its mechanical stability. However, an FS equal to one is not sufficient, as any defects in the material can lead to failure. Therefore, a factor of safety greater than one is commonly employed, typically in the range of 1.5 – 2 for CPB (Li, 2015). Since the material strength-based design approach is able to guide the engineering design and assessment of mechanical stability of CPB mass, this design method plays a critical role in the successful implementation of CPB technology in practice.

The fracture toughness is used to measure the strength of a material when it has a pre-existing defect. This measure is highly applicable to CPB due to the nature of its application. CPB is often poured against the wall of a mine, which is a rock with unsmooth and random geometries. In this case, some cross-section of the CPB stope will be thin relative to the rest of the stope. It is at these points that a pre-existing defect is naturally introduced into the material. These points are the most likely to fail, so the need for understanding the behavior of these materials is clear.

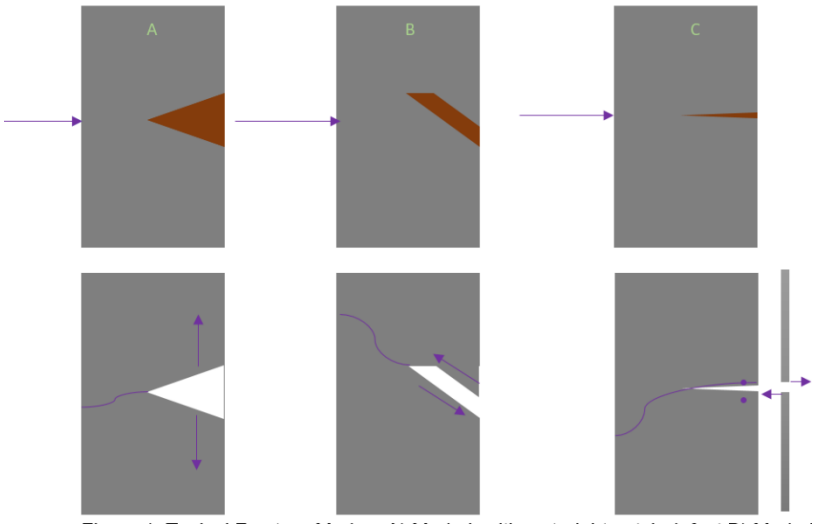

Figure 1.1: Types of fracture behavior (A) Mode-I, (B) Mode-II, and (C) Mode-III.

To employ the strength-based design method, the unconfined compressive strength (UCS) is widely adopted to determine the FS (Xu et al, 2019). This is because CPB mass commonly acts as pillars in stopes and is mainly subjected to compressive stress. Correspondingly, the compressive behavior of CPB has attracted considerable attention. It has been confirmed that the cement hydration process dominates the development of UCS with curing time (Benzaazoua et al, 2003). Cement hydration refers to the chemical processes among cement and water. Based on the previous studies (Qi and Fourie, 2019; Jafari, 2020), several reactions occur in multiple stages and are split based on the focus of the study. The first of these stages is a result of C_3S dissolving and having an exothermic reaction with water, known as the initial dissolution stage. While the induction stage is not well understood, it is beneficial to exist as it improves the workability of the cement mix. In the acceleration stage, the cement starts to crystallize, forming C-S-H (calcium silicate hydrate) crystals, as well as calcium hydroxide (CH). During the deceleration stage, the smaller C_3S particles have completely reacted, while larger grains are surrounded by the precipitated hydrates. In the final stage, slower reactions, such as C_2S hydration occur. The initial stages are especially important, as the early-age strength is important for the applications of CPB. Therefore, it is imperative to improve the early-stage strength of CPB. The water content of CPB is also a key

factor in the hydration process. While improving the cement content is important, the water content also plays a key role in the cement hydration.

1.2 Problem statement

The key factor which influences the strength of CPB is the mix design. CPB consists of three main ingredients: tailings, binder, and water. The tailings compositions vary depending on where they were obtained. Therefore, the factors which can be controlled are the cement and water content.

The use of cement as a binder accounts for around 75% of CPB costs (Carvalho et al, 2017, McLellan et al, 2011). The most common binder is Ordinary Portland Cement (OPC). Therefore, the optimization of cement use is very important as a cost-saving measure. However, cement content plays a key role in the CPB strength (Sheshpari, 2015, Tariq and Yanful, 2013). In addition, the cement content is important for the workability of CPB, which is typically piped from the surface to the stope location. It has been confirmed that the cement hydration process dominates the development of UCS with curing time (Benzaazoua et al, 2003).

Water is used to activate the hydration reaction of cement. The water to cement ratio is very important in cementitious materials. More water will lead to a more workable material, however it will have lower strength. Meanwhile, a lower water content, and therefore higher solids content, ensures a better strength, but the material will be less workable (Li et al, 2020). This logic also applies to CPB mixes that depend on cement. Therefore, the choice of water content is important to the design of CPB. One additional concern is that often, tailings come from a tailings pond, and while they are dewatered, they still contain some water content. Therefore, in the lab setting, where dry artificial tailings are used, more water must be considered.

1.3 Research methodologies

In order to examine the fracture behavior of CPB, a series of fracture toughness tests will be performed. The fracture tests consist of two types of tests, including the semi-circular bend (SCB) tests and the end-notch disk bend (ENDB) tests. SCB tests are utilized to study the fracture

behaviors of CPB under mode-I and mode-II loading conditions, and ENDB tests are employed to investigate the mode-III fracture behavior.

Two influential factors, including chemical and hydraulic factors, are incorporated into the testing program. The study on the chemical factors focuses on the effect of cement content (Cc), and three cement content, including 2%, 4.5%, and 7%. In terms of hydraulic factors, the water-to-tailings ratios (including 0.33, 0.36, and 0.39), drainage conditions (including drained and undrained CPB samples), and resaturation conditions (CPB samples are re-saturated at the targeted curing time). The water-to-tailings ratio (WTR) is used to measure the mass of water in comparison to the mass of tailings in the mix. The reason to use this measure, as opposed to the more common water-to-cement ratio is to prevent changing the Cc when increasing the initial water content. This allows for checking the effect of Cc and initial water contents separately.

In addition, a series of auxiliary tests are to be performed on CPB samples. Specifically, the gravimetric water content of CPB will be measured. Meanwhile, some tests will be performed to determine the degree of saturation and porosity of CPB samples. Finally, CPB sample will be examined using a scanning electron microscope (SEM), to observe the microstructure of the samples.

1.4 Thesis organization

This thesis consists of five chapters to demonstrate the research work and findings. In Chapter 1, the background information and research methodology are presented. Chapter 2 is used to summarize the current literature on CPB materials, including three sections. First will be the background information of CPB technology. Following that will be a discussion of microstructure considerations, and then conventional geomechanical behaviors of CPB. Chapter 3 will cover the experimental methods used to prepare and test the samples. In addition, it covers the methods used to perform auxiliary tests such as the SEM analysis, GWC, porosity, and saturation. Finally, the method to calculate the properties of CPB will be shown in Chapter 3. In chapter 4, the results from the experimental study will be discussed to reveal the effect of cement content and various hydraulic factors on the fracture behaviors and properties, including fracture toughness, stiffness, and work of crack initiation of CPB under mode-I, mode-II, and mode-III loadings. Finally,

chapter 5 will be used to present conclusions, and provide recommendations for future work in the area.

Chapter 2 Literature review

2.1 Background

CPB commonly uses OPC as the binder, which is the main driver behind the chemical process. The chemical composition of OPC based on chemical analysis is shown in Table 2.1. The chemical composition of a material can be determined through the use of X-Ray Fluorescence (XRF) (Qi and Fourie, 2019). OPC chemical composition is important to note as it plays into the reactions for CPB. There are four major mineral phases that constitute the makeup of OPC (Ylmén, 2013). Alite (Ca_3SiO_5) is the preferred phase in OPC in the presence of excess CaO, and can form stably above 1250°C (Benmohamed et al, 2016), and composes 50-70% of OPC weight (Ylmén, 2013). It appears with a variety of crystal sizes, as well as morphology. The crystal edges appear clearly while having amorphous phases. Belite (Ca_2SiO_4) forms at temperatures of 900-1250°C, and involves the reactions of CaO and SiO_2. It accounts for 15-30% of the weight of OPC. The formation of alite and belite phases are inversely proportional; with higher alite contents, the belite content will decrease. The crystal structure of belite is difficult to identify. Belite has a relatively slow reaction when compared to alite, and does not significantly contribute to early-age strength of CPB (Ylmén, 2013). However, past the 28-day mark, it adds significantly more strength. Aluminate ($Ca_3Al_2O_6$), and Ferrite ($Ca_4Al_2Fe_2O_{10}$) occur in smaller amounts compared to the other mineral phases. Aluminate appears as an interstitial phase, composing 5-10% of weight. After curing, the presence of aluminate can lead to further reactions with water, leading to rapid settling. Ferrite composes 5-15% of OPC weight, and its rates of reaction vary (Ylmén, 2013). These phases are not always pure, which explains the variance found in chemical composition by study. To simplify reaction equations, several shorthand nomenclature have been adopted for these minerals; those being C = CaO; S = SiO_2; A = Al_2O_3; F = Fe_2O_3; S^{-} = SO_3 H = H_2O.In this way, Alite can be represented by C_3S, Belite as C_2S, Aluminate as C_3A, and Ferrite as C_4AF.

Table 2.1: Composition of OPC.

Chemical	Zhai et al (2021)	Asgari et al (2016)	Bohac et al (2016)	Liu et al (2019)
SiO_2	22.63	22.2	24.01	19.19
CaO	60.52	65.65	64.48	64.13
Fe_2O_3	4.74	2.85	2.97	3.33
Al_2O_3	4.27	4.71	7.42	4.50
MgO	3.26	1.95	2.67	1.82
K_2O	1.22	0.48	0.77	1.04
SrO	-	-	0.03	-
MnO	-	-	0.22	-
TiO_2	-	-	0.32	0.24
Na_2O	-	-	0.26	0.41
SO_3	3.26	-	3.26	1.06
P_2O_5	0.03	-	-	-
Na_2O_3	-	0.16	-	-

The classification of OPC hydration stages depends are typically identified by the heat released during the hydration process (Qi and Fourie, 2019). A typical heat release versus time graph is shown in Figure 2.1, which can be obtained through laboratory measurements. The first of these stages is known as the dissolution stage. This stage is characterized by a quick reaction between the cement material and the water. This phase occurs rather quickly, releasing a large amount of heat. One interesting difference in CPB is that, unlike most cement-based materials, the electrical resistivity continues to rise while it would usually fall (Liu et al, 2019). The cause of this must be attributed to a physical phenomenon, as it does not change the hydration heat. The second stage is characterized by a large drop in heat and a reduction in the dissolution rate of minerals. Known as the induction stage, the mechanisms are not fully agreed upon. However, it is believed that the existence of this phase improves workability. Next is the acceleration stage, which is characterized by the nucleation and growth of new crystals. C_3S and little C_2S become C-S-H crystals, which gives the major strength improvement in CPB. The heat released at this point increases quickly

until the next stage. Generally this is the end of the early phases of cement hydration, which occurs around 10-20 hours after initial mixing. The deceleration stage occurs over a much longer period of time compared to previous stages. At this point, the smaller particles of cement have reacted completely, and surround larger particles. The stage sees a gradual drop in heat flow over a significantly longer period compared to the previous three stages. The slow reaction stage is effectively a continuation of this trend, with a very slow reduction in the heat flow. It is here that many of the unreacted minerals begin to hydrate, such as C_2S.

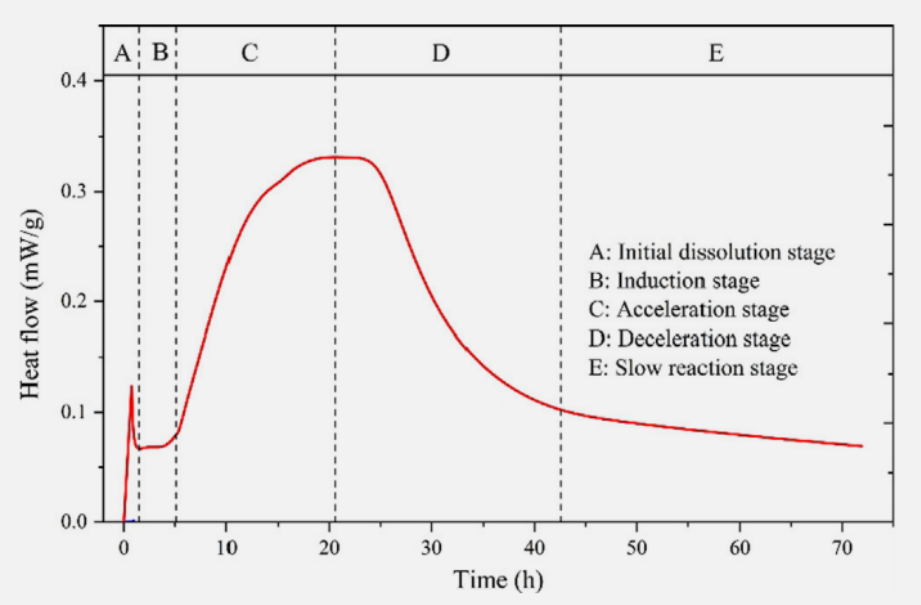

Figure 2.1: Heat flow of CPB with time (Qi and Fourie, 2019).

2.2 Microstructure Analysis

In order to understand the effects that the hydration process has on the microstructure of CPB, several tools can be used. The first of these is scanning electron microscope (SEM), which allows for imaging of CPB samples at scales as small as 1nm. SEM uses electrons scattered off the sample to create images; it can also be used for chemical analysis through x-rays. The test can be performed by forming several test cylinders of CPB, allowing them to cure for differing periods before analyzing the specimen using SEM. To that end, several studies have been performed using this technique. While SEM allows for the direct imaging of CPB microstructure, it does not directly

describe the characteristics (Liu et al, 2019). Therefore, analysis of SEM data can be done using additional software. Analysis can also be done through visual inspection of the processed image. As shown in Figure 2.2, the microstructure of CPB changes with curing time (Cheng et al, 2019). At three days of curing, the CPB is denser with needle-like structures known as ettringite, which are between clusters of C-S-H. Meanwhile, at seven days, the C-S-H clusters are much larger but have yet to form a cohesive product. After 28 days curing, there are less pores and they are relatively smaller. As the CPB reaches longer hydration times, it can be seen that the bonds form within the CPB, as the hydration products continue to form. C-S-H forms and holds together ettringite as well as calcium hydroxide crystals, which appear as flake-like crystals. In Figure 2.2-B, the effects of changing the cement contents can be seen. When the cement content is increased, the C-S-H is composed of larger flocs, and gives way to a more structured, dense network with more calcium hydroxide crystals. While it can be concluded that a higher cement to tailing ratio (1:4) increases the size and density of hydration products, it does not accurately represent CPB practice, which uses lower cement to tailing ratios.

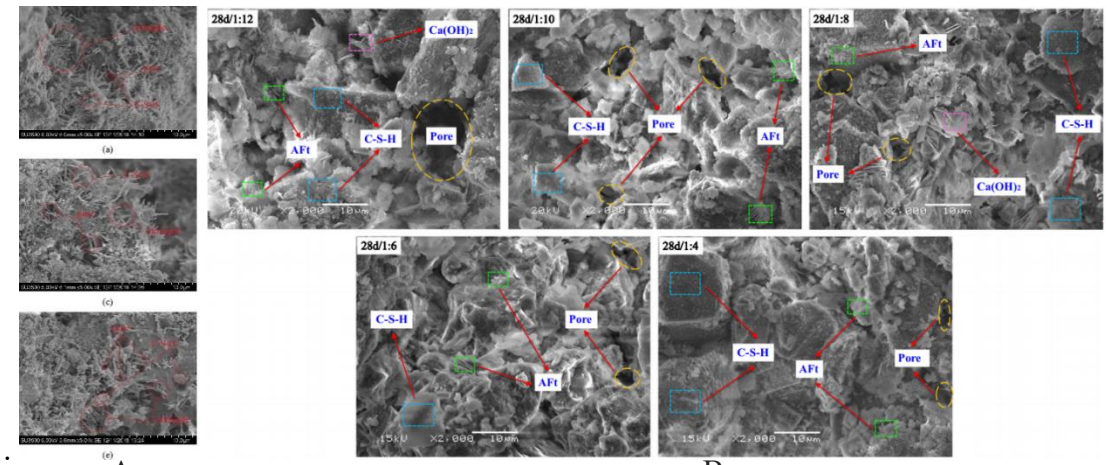

Figure 2.2: SEM Images of CPB. a) hydration time (Chen et al., 2019) b) cement-tailing ratio (Liu et al., 2020).

Another tool that is available to measure the microstructure of CPB is Mercury Intrusion Porosimetry (MIP). By using a liquid that does not wet a surface (i.e., The contact angle is greater than 90°), the liquid only enters pores when pressurized (Abell et al., 1998). Since the relation

between the pressure and capillary diameter is known, the pore characteristics can be characterized using such a liquid such as mercury. Using this technique allows for the measuring of porosity of CPB while the hydration occurs. While porosity can be observed using SEM, direct measurement is not possible. In Figure 2.3, the maximum volumetric water content; that is, the maximum pore space; occurs between three and eight hours into curing, even while changing the binder or temperature. As the curing continues, the pore structures begin to close as the volumetric water content decreases.

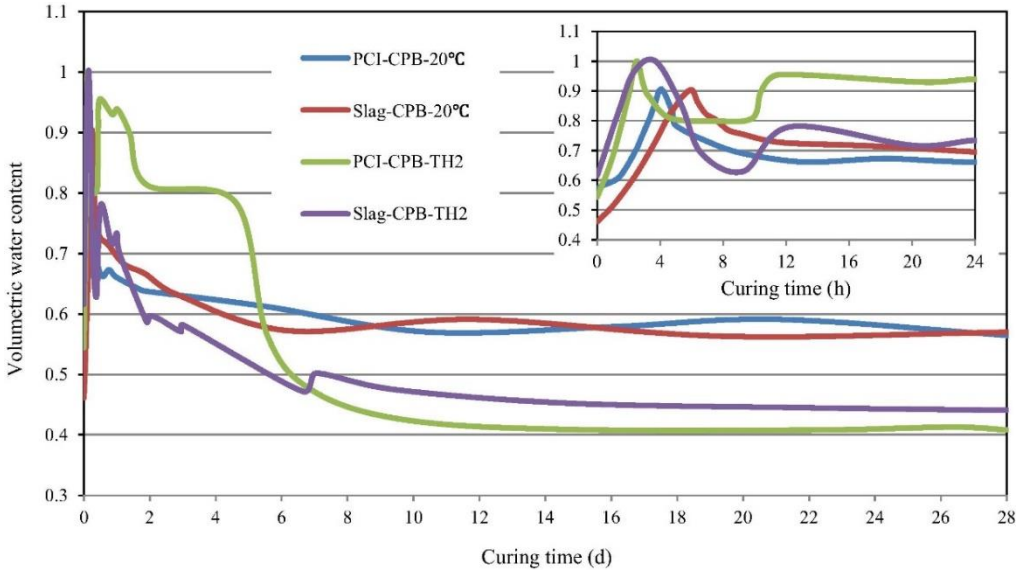

Figure 2.3: Volumetric water content with curing time (Tian and Fall, 2021).

2.3 Evolutive mechanical behavior and properties of CPB

While a good understanding of the microstructure provides key insights into CPB behavior, a macroscale approach must also be considered. The changes in macroscale behaviors with hydration can be useful in predicting material properties of CPB, which are needed for design. In particular, three macroscale properties will be examined, including compressive, tensile, and shear behaviors. The effects of hydration include hydration time, curing/confining stress, and temperature.

2.3.1 Compressive Behaviour of CPB

Many tests can be used to assess the compressive strength of CPB. The most ubiquitous test of CPB compressive strength is UCS due to its convenience and low cost (Xu et al., 2019). UCS test consists of casting a cylinder of CPB, which is loaded into a testing cell. The loading cell progressively applies force to the cylinder until the sample fails. The applied stress from the loading cell is the compressive strength of the CPB. By performing this test on samples that have been cured at different times, the effects of hydration on CPB strength can be determined. The study by Xu et al. showed the effect of hydration time on CPB under varying curing temperatures. The UCS was done under zero confining pressure conditions. In all cases, the UCS of CPB improved with a longer hydration period. In addition, increasing the cement content improves UCS significantly (Zhou et al., 2019). When the CPB cures under stress, it was found that significant improvements to the UCS were shown, as shown in Figure 2.4. In addition, Figure 2.4 shows the effects of increasing temperature on UCS. The improvement in CPB due to temperature is attributed to the self-desiccation effect because of the reduction in pore water pressure due to accelerated hydration (Tian and Fall, 2020). This effect can also improve CPB resistance to liquefaction.

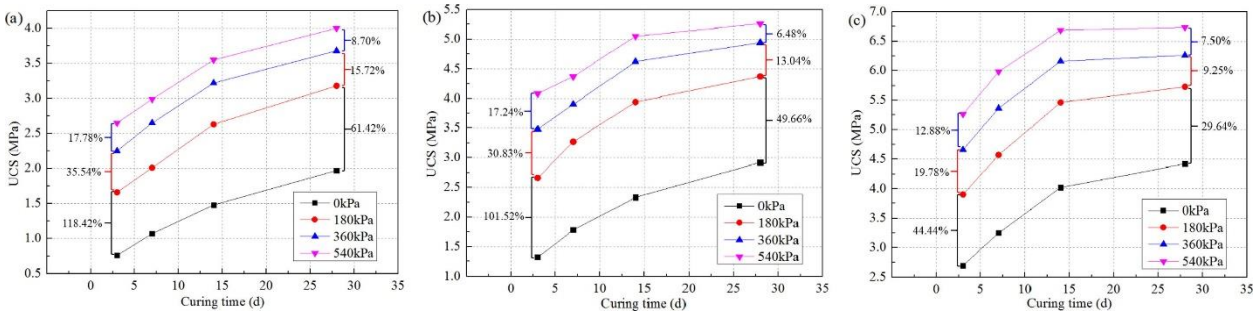

Figure 2.4: UCS improvement with higher curing stress under a) 20 °C, b) 35 °C, c) 50 °C (Shunman et al, 2020).

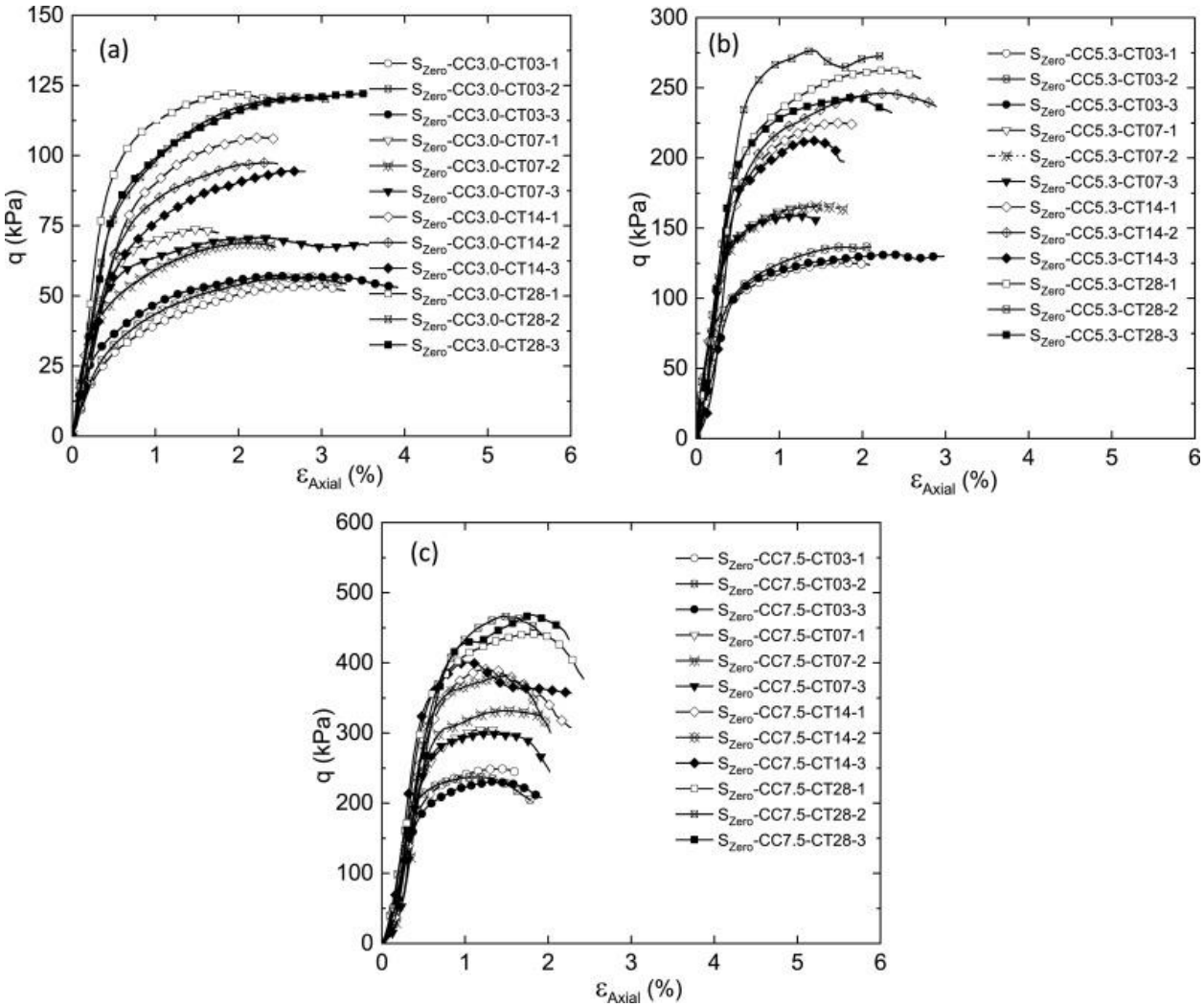

Figure 2.5: CPB Stress-strain curves at a) 3% cement content, b) 5.3% cement content, and c) 7.5% cement content (Jafari and Grabinsky, 2021).

While UCS can give insight into the properties of CPB, a complete picture of CPB behavior can be determined using the triaxial test. The test uses a rig that can apply both compressive force as well as a confining pressure. The triaxial test can provide a stress-strain graph to analyze the full behavior of CPB. Jafari and Grabinsky (2021) looked at the failure of CPB with low sulfide content. They also compare the properties based on curing time and cement content, as shown in Figure 2.6. With regards to the increase in curing time, the samples with longer hydration time withstood higher stress before failure. The shape of the stress-strain curve is nonlinear, with the

stress increasing mainly at strains below 1%. However, the peak strain is not constant for all CPB mixes (Fall et al., 2007). At 3% cement content, the peak stress occurred after significant strain. Then, as material failure begins to occur, the stress reduces before compressive failure, around 4-5% strain. As the cement content increased, the peak stress achieved for all curing times is much higher. While the pre-peak behavior is similar to lower cement contents, the post-peak curve occurs over a lower strain. Failure occurs at 2-3% strain for 5.3% cement content, and around 2% at 7.5% cement content. They found the typical stress-strain curve of CPB to follow this nonlinear curve. Fall et al. (2007) tested approximately eighty samples of CPB with various curing times between seven and 120 days.

Fall et al. (2007) also discuss the elastic modulus of CPB. CPB subject to confining pressure has a differing elastic modulus to those without confining pressure. In general, increasing the confining pressure decreases the elastic modulus. This effect becomes more pronounced as the UCS of the CPB increases. The elastic modulus also improves with an increase in cement content.

2.3.2 Tensile Behaviour of CPB

The tensile strength of CPB is important for the creation of stable stopes, especially in self-supporting spans. It is well known that the tensile strength of cement products is much lower compared to compressive strength. In addition, the tensile behavior of CPB is not well explored. Direct tensile testing for CPB is difficult, as the lower strength makes it difficult to prepare the specimen (Pan and Grabinsky, 2021), which is best shaped as an axisymmetric dogbone. Therefore, the commonly used test is the Brazilian Split test, which is an indirect tensile test. The test consists of a loading cell with a Linear Variable Differential Transformer (LVDT), which measures the displacement (Jafari and Grabinsky, 2021; Komurlu et al., 2016). The equipment needed is the same as compressive testing. While this test is easier to perform, it does not provide accurate information on the elastic parameters of CPB in tension (Pan and Grabinsky, 2021). In addition, CPB can be subject to crushing in this test. Therefore, both the indirect and direct method results will be discussed.

As the indirect test is easy and inexpensive to set up, many different tests can be run. By adjusting the loading plate, several loading conditions can be tested. For example, by changing the loading apparatus, the load distribution can be changed to observe different results, such as using flat plates or angled loads. As seen in Table 2.2, the changes in loading cell give different tensile strengths for the same sample. In addition, the figure shows that increasing the cement content has a significant effect on the tensile strength. Meanwhile, the higher curing age also had a significant effect for the higher cement content CPB. At the low cement content, curing age has a minimal effect on strength. In general, the samples with lower curing time and lower cement content tend to show multiple cracks during testing. Meanwhile, the stronger specimens tend to fail with a single, central crack.

Table 2.2: Average indirect tensile strength of CPB (Komurlu et al, 2016).

w-c ratio	Curing Time	Split Jaw	Flat	15°	30°
75%	2 days	2.81	2.69	2.06	2.65
75%	14 days	4.37	2.69	2.72	4.67
235%	5 days	0.22	0.19	0.15	0.19
235%	28 days	0.29	0.22	0.21	0.31

The study by Pan and Grabinsky (2021) aims to perform an effective direct tensile test on CPB samples. It appears that the tensile behavior of CPB is linear, regardless of cement content or curing time. From these results, it is clear that an increase in cement content leads to an improvement in the tensile strength. In addition, a longer curing time improves the tensile strength. The majority of samples failed at or near the midspan.

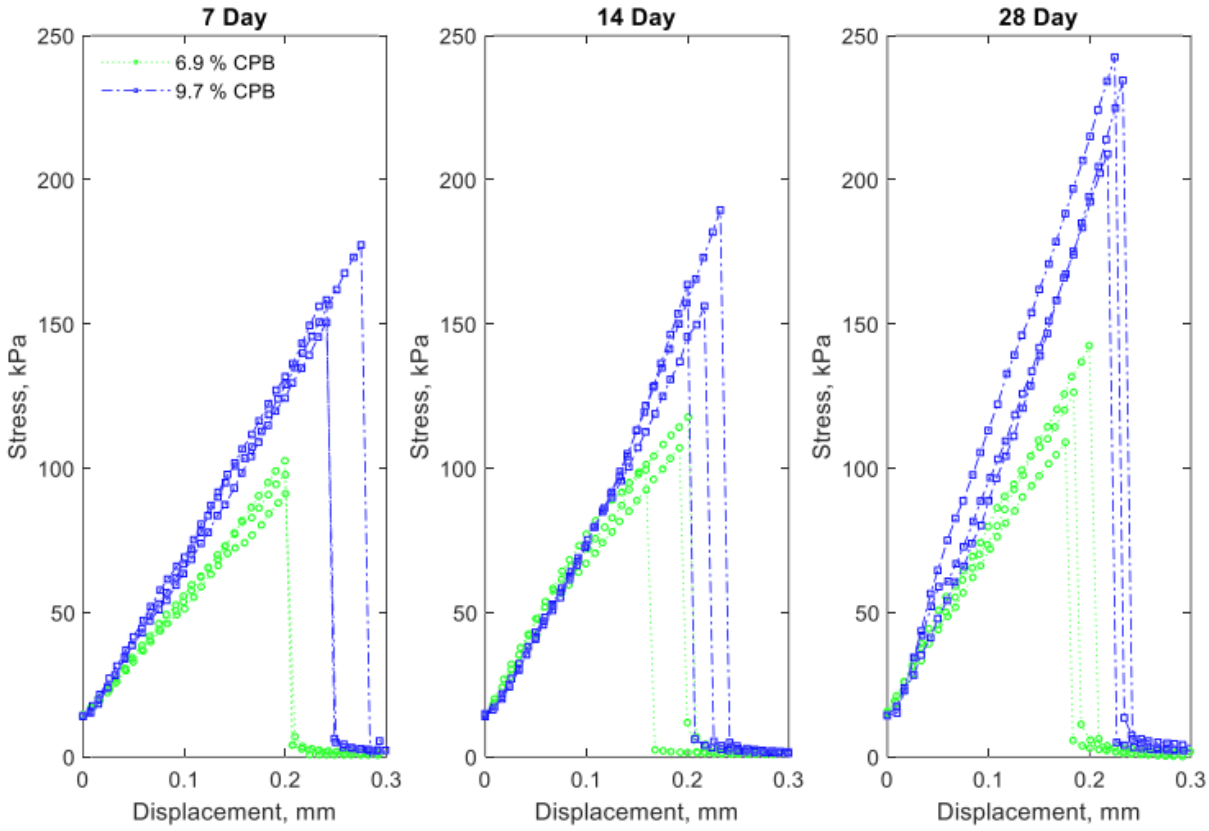

Figure 2.6: Direct Tensile Stress-Strain Curve (Pan and Grabinsky, 2021).

2.3.3 Shear Behaviour of CPB

The characterization of shear stresses in CPB is important to design. In mining stopes, the CPB interface with the adjacent stope depends on shear strength (Xiu et al., 2021). In the early stages, CPB acts as a non-newtonian fluid having no shear strength (Jafari, 2020). As the CPB cures, it gains shear strength as the chemical bonds form. The direct shear test can be used to analyze the shear strength of CPB and the CPB-rock interface. This test places the sample into a shear box, which has a seam in the center. A loading cell applied load to the top half of the shear box while the box was restrained. The load is increased continuously until failure, LVDTs can be used to measure the displacement of the sample. For CPB-rock interface, the CPB is in one half of the box, while the rock sample is placed in the other half. Therefore, the failure occurs along the interface.

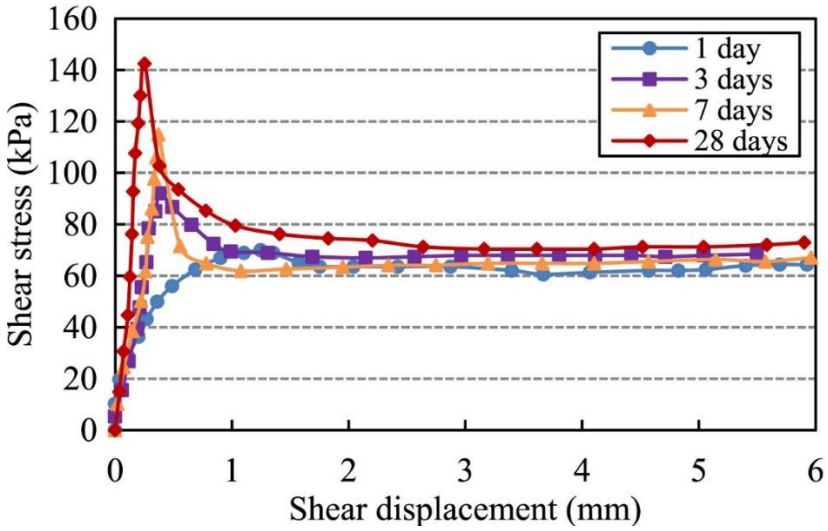

Figure 2.7: Curing time effect on shear stress (Fang and Fall, 2018).

Fang and Fall (2018) performed such a test using granite samples and CPB. In addition, the pore pressure of CPB was monitored. As shown in Figure 2.7, the sample initially experiences high stress and reaches its peak very quickly. Afterward, the material experiences a slow decline in stress until it approaches residual stress. The higher curing time resulted in a higher peak shear stress, which appears to occur close to the 0.5mm displacement. However, at the curing times of one day, the peak stress is also the residual stress. Notable is that the samples converged around 60-70 kPa residual stress regardless of the curing time. If the curing temperature is also considered, at higher temperatures, the CPB cures more effectively due to accelerated hydration.

While the direct shear test is easy to use for studying the mechanism of CPB-rock interface, including stress distribution and size effect (Weilv et al., 2021). Therefore, an alternative is to use a triaxial test. This allows for more varied tests, such as changing the interface angle. Weilv et al. (2021) found that shear properties of CPB are changed when interface angle is taken into account, as seen in Table 2.3. The failure in CPB-rock differs depending on cement content. As the cement content increases, the failure mode changes from bulging deformation to shear slipping. With regards to the hydration effect, Xiu et al. (2021) found that as the hydration time increased, the peak shear stress of CPB-rock interface increased significantly. As the slipping failure surface is

at the interface, it was found that the wet rock surface significantly reduced the cohesion, while the friction angle was slightly higher.

Table 2.3: Shear parameters based on interface angle

Cement content (%)	CPB		CPB-rock specimen (α = 60°)	
	Friction angle ϕ_0 (°)	Cohesion c_0 (kPa)	Friction angle ϕ_p (°)	Cohesion c_p (kPa)
2.5	35.62	19.84	36.71	14.96
5	36.03	33.53	35.67	25.72
7.5	36.2	68.83	38.51	13.68

It is also possible to measure the shear strength of CPB without consideration of the CPB-rock interface. Araujo et al., 2016 used differing confining pressures, curing periods, cement content, etc. Among their findings, it was reported that the self-consolidation process of CPB is key to gaining high strength. Of note is that the samples with no consolidation showed a similar void ratio to samples in-situ. Further studies to determine if this effect occurs in-situ are needed to confirm these phenomena. The specimens which were allowed to self-consolidate during the first 24 hours of curing were 23% stronger than those that did not. In addition, it was found that high confining pressures were beneficial for CPB, so long as pressure was gradually increased to prevent crushing the specimen. Of note is that difference in strength between the 28-day old specimens and 100+ day old specimens was not significant. Therefore, it is acceptable for studies to focus on 28-day strength of CPB.

Chapter 3 Experimental testing program

3.1 Materials

The main material used for this study is the artificial tailings, which consist of 98% pure silica powder. The artificial tailings were chosen due to the ease of access and the consistency of the material. Due to the tailings being an inhomogeneous material, it can cause variance in the results. To bind the artificial tailings, ordinary Portland cement (OPC) is used. The tap water in the lab is used to mix the ingredient together.

3.2 Mix recipe and curing method

The mix recipe will be varied for each test in order to determine the effects of cement content (Cc) and hydration on fracture toughness. The mix recipe was determined by using the specified Cc for each sample. Based on the volume of the curing cylinder, and an assumed density of CPB of 20 kN/m^3, the mass of the sample could be determined. Then, the mass of cement, water, and tailings to use can be calculated using several equations. To determine the mass of cement, two equations are used to substitute out the other variables. Then, Equation 3.4 can be used to determine mass of tailings. Finally, using the water-to-tailings ratio, the mass of water was determined. A summary of the mix design for each sample is provided in Table 3.1.

The cylindrical molds have dimensions of 20 cm in height and 10 cm in diameter. Therefore, the volume of the mold is calculated as:

$$V = A*H = \pi r^2 H = \pi*5^2*20 = 1570.8\ cm^3 = 0.0015708\ m^3 \quad (3.1)$$

Where

A is the area of the mold cross-section, which is circular. $A = \pi r^2$ [cm^2]

H is the height of the mold [cm]

V is the total volume of the mold [cm^3]

Assuming a density of CPB, Y_{CPB} equal to 20 kN/m^3, the mass of CPB is

$$M = Y_{CPB} * V = \frac{20*1000}{9.81}[kg/m^3] * 0.0015708[m^3] = 3.202kg \quad (3.2)$$

Where,

M is the mass of CPB in the sample mold [kg]

The cement content of CPB can be determined by

$$C_C = \frac{M_C}{M_C+M_T} \quad (3.3)$$

Where,

Cc is the percent of cement content in the mix, by weight

M_c is the mass of cement [kg]

M_T is the mass of tailings [kg]

Rearranging for M_T,

$$M_T = M_C\left(\frac{1}{C_C} - 1\right) \quad (3.4)$$

$$\text{WTR} = \frac{M_W}{M_T} \quad (3.5)$$

$$M = M_C + M_T + M_w = M_C + M_T + (WTR)M_T \quad (3.6)$$

where,

M_w is the mass of water [kg]

Substituting Eq. 3.4 into Eq. 3.5,

$$3.202 = (1 + WTR) * M_C\left(\frac{1}{C_C} - 1\right) + M_C \quad (3.7)$$

Where $C_c = 0.045$, so

$$3.202 = 1.36 * M_C \left(\frac{1}{C_C} - 1 + 1\right) \tag{3.8}$$

$$M_C = \frac{3.202}{1.36} C_C = 0.10596kg \tag{3.9}$$

$$M_T = 0.10596 \left(\frac{1}{0.045} - 1\right) = 2.24877kg \tag{3.10}$$

$$M_w = 0.36 * 2.24877 = 0.80956kg \tag{3.11}$$

Using these numbers, the actual CPB mass is slightly lower than assumed. However, the WTR and C_C are correct, which is the most important values for these tests. In addition, the values were scaled down to prevent material waste, as the different mixes have differing densities.

Table 3.1: Mix recipe for preparation of CPB samples.

Factor	Effect of cement content			Effect of hydraulic factors				
Group	1A	1B	1C	2A	2B	2C*	2D*	2E*
WTR	0.36	0.36	0.36	0.33	0.39	0.36	0.36	0.36
Cc(wt%)	2	4.5	7	4.5	4.5	4.5	4.5	4.5
M_c (g)	47.1	106	164.8	0.11	0.1	106	106	106
M_t (g)	2307.6	2248.8	2189.9	2299.5	2200.2	2248.8	2248.8	2248.8
M_w (g)	830.8	809.6	788.4	0.76	0.86	809.6	809.6	809.6

To prepare the CPB, the dry ingredients are first mixed in a bowl. Then, the water is slowly added, using a spatula to minimize spills and mix the materials together. While the dry ingredients are mixed, a very small excess of material was added to account for the loss due to the dust and vapor from the water mixing. The mixed ingredients are then transferred to a variable speed mixer. This mixer was chosen for its blade, which can mix the entire sample evenly, and for the variable speed controls. Once the bowl is set, the mixer is set to the lowest speed and runs for ten minutes. Five minutes in, the mixer is stopped, and a spatula is used to scrape the sides of the bowl into the center. This is done to ensure even mixing. Next, the CPB is transferred into the sample cylinders for curing. After the cylinder is filled, each side is tapped with a rubber mallet six times to remove

air bubbles, for a total of 25 taps. The spatula is used to ensure surface control. Finally, the top of the cylinder is covered and stored until the appropriate test date.

In order to examine the drainage effect on CPB, sample set 2C was prepared using a mold with a hole of at least 1.5mm diameter pierced through before the casting. The samples were allowed to cure on a solid wood surface. Significant drainage was observed during the first hours of curing, after which the sample hardened, plugging the drainage hole.

Samples 2D and 2E had additional special curing conditions. While these two sets were cured in a similar fashion to the other sets, they underwent special procedures before testing. Sample 2D was subjected to a resaturation process. This was accomplished by placing the freshly demolded samples into a vacuum chamber, which is filled with water. The vacuum chamber was run for a minimum of one hour, reaching a negative pressure of 29 mmHg. Due to the backflow protection system, a slight pressure loss was noted. However, this was necessary to prevent water damage to the pump. In addition, the pressure loss was quite low, and to compensate, extra time in the vacuum tank was allowed. The process of resaturation was borrowed from Libos and Cui (2020), which confirmed its effectiveness. The equipment (Figure 3.1) used was identical to the Libos and Cui method, with the addition of the backflow protection. Once resaturation was complete, the samples were cut and protected with plastic wrap to avoid evaporation. The samples were unwrapped individually as they were tested. The reason these samples were resaturated, as opposed to curing in water, was due to the fact that the CPB is very soft.

For samples from set 2E, the samples were demolded and cut as specified previously. Then, to remove any water contents, the samples were dried in an oven for 24 hours at 110 °C before undergoing mechanical testing.

Figure 3.1: The vacuum pump system used in resaturation.

3.3 Mechanical testing

To prepare the samples for fracture testing, the cylinders are cut into the proper shapes. The samples are first removed from the cylinders using a hydraulic air hose. The cutting process was performed using a circular table saw. To ensure the consistency of samples, at least 1 cm of each end of the sample is removed. The cylinder is sliced into three disks, each with a 5 cm thickness. Often, an extra length of the specimen is left over. If it is not significantly damaged, the extra piece was used for the auxiliary testing. Safety goggles and masks were required during the cutting process in order to protect from the dust produced. A visual representation of the process is shown in Figure 3.2. The final notched samples are seen in Figure 3.3

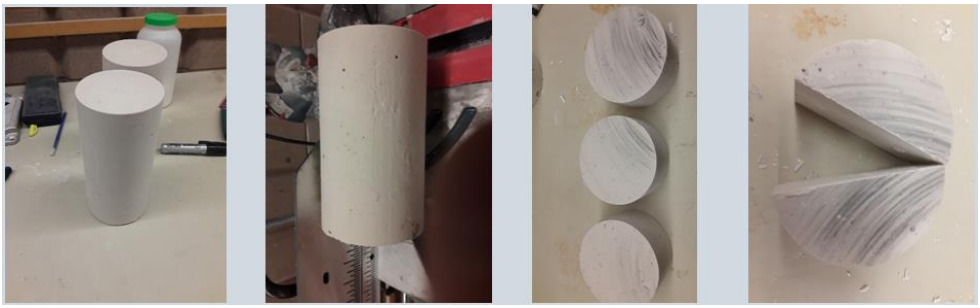

A B C D

Figure 3.2: Sample cutting process.

(A) Mode-I sample (B) Mode-II sample (C) Mode-III sample

Figure 3.3: CPB sample under (A) mode-I loading, (B) mode-II loading, and (C) mode-III loading.

For Mode-I and II fracture, the disk samples are cut into semicircles with a diameter of 10cm, as shown in Figure 3.3-A and 3.3-B. A 2.5 cm notch is cut into each sample based on the mode, with Mode-I having the vertical notch and Mode-II having the angled notch. This method is the SCB test. In order to test, the samples were loaded into a custom frame, as shown in Figure 3.5. The loading rate was displacement-based, using a rate of 1mm/min.

For Mode-III fracture, the ENDB test is used. This involves cutting the notch into a full circular sample and angling the notch at 60 degrees relative to the loading bar, as shown in Figure 3.3-C. As a result, each cylinder was able to produce six samples for testing. While a few samples were damaged, at least three tests were performed on each sample.

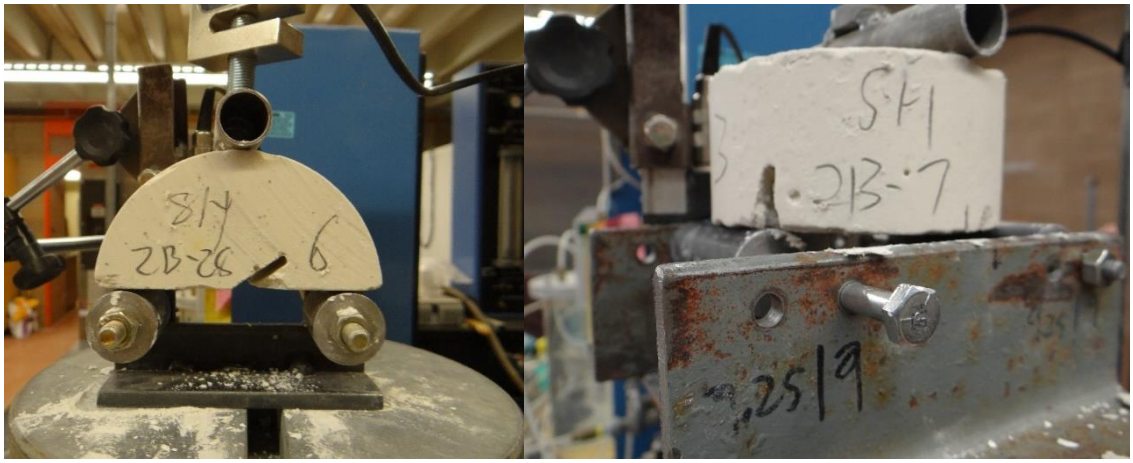

Figure 3.4: Load frames for SCB (left) and ENDB (right) tests.

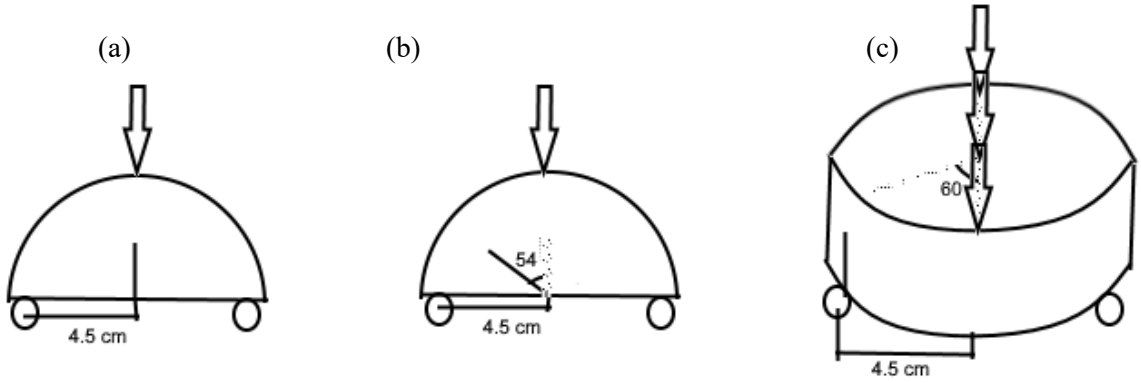

Figure 3.5: Testing setup for Mode I (a), Mode II (b), Mode III (c)

3.4 Auxiliary analysis

The void ratio and degree of saturation were determined as according to *Using Thermal Profiles of Cemented Paste Backfill to Predict Strength* (Mozzaffaridana, 2011). In order to calculate these values, first, a portion of each sample was weighed with a small string attached. After recording the original weight, the samples are dipped in a paraffin wax with a density of 0.8 g/mL. The sample is again weighed after the wax hardens and is then hung from a hook, submerged in water. The submerged specimen's weight is determined. The final piece of information needed is the water content. Using different samples, they are first weighed and then dried for a minimum of 24

hours. The dried weight of the sample is determined, and the difference between these two values is the weight of water. The gravimetric water content (GWC) is the weight of water divided by the dry weight of soil. Once all of this information is collected, the calculations can be performed as specified by Mozzaffaridana (2011). Note that, for tests 2D and 2E, the degree of saturation is at 100% and 0%, respectively.

Another auxiliary test performed was the SEM analysis. A Hitatchi SU-70 model, with a resolution of 1nm. In order to image the samples, first each sample is dried at 45 °C for 24 hours. The samples are stored in an airtight plastic bag until ready to test. When ready, a 5mm diameter section is cut and glued to a stand. Up to six of these samples can be loaded simultaneously. Before entering the vacuum chamber of the SEM, the samples are coated with gold in order to improve the reflectivity for the electrons. Once the samples are loaded, and the chamber reaches a sufficient vacuum, the proprietary software can be used to view and image the CPB microstructure.

3.5 Determination methods of fracture properties

The fracture toughness can be determined based on the following equations.

$$K_I = \frac{P}{DT} Y_I \sqrt{\pi a} \tag{3.11}$$

where

P is the maximum force (peak value of force vs. displacement curve) (N)

D is diameter of semicircular specimen (m)

T is the thickness of semicircular specimen (m)

a is the notch depth (m)

Y_I is the normalized stress intensity factor for Mode-I (dimensionless)

$$K_{II} = \frac{P}{DT} Y_{II} \sqrt{\pi a} \tag{3.12}$$

where

Y_{II} is the normalized stress intensity factor for Mode-II (dimensionless)

For these samples, a = 0.025 m, D = 0.102 m, T = 0.05 m, Y_I = 6.52 and Y_{II} = 1.072. Therefore, the equations reduce to:

$$K_I = 365.445P\ \left[Pa\sqrt{m}\right] \tag{3.13}$$

$$K_{II} = 60.086P\ \left[Pa\sqrt{m}\right] \tag{3.14}$$

Mode-III samples are prepared by cutting a notch into a full disk, as shown in Figure 3.4-C. The samples are loaded into a testing rig, again with a displacement rate of 1mm/min, and the force-displacement curve is logged. The fracture toughness, K_{III}, is calculated using the following equation.

$$K_{III} = \frac{6PS}{RB^2} Y_{III}\sqrt{\pi a} \tag{3.15}$$

where

a: the notch depth (m)

B: thickness of the disc specimen

S: the horizontal distance between central and edge bars

R: radius of the disc specimen

β: inclination of notch line w.r.t. the central bar

Y_{III}: is the normalized stress intensity factor for Mode-III (Y_{III} = 0.0713)

For this calculation, a = 0.02 m, B = 0.05 m, R = 0.05 m, S = 0.045 m, β=60°, and Y_{III} = 0.0713. The equation then reduces to:

$$K_{III} = 38.604P\ \left[Pa\sqrt{m}\right] \tag{3.16}$$

The fracture equations are now in the form of a linear scale factor of the peak force. Once the peak force is determined through mechanical testing, the fracture toughness can be easily calculated.

Another measure of the change in CPB is the work of crack initiation. To determine this value, one must calculate the area under the load-displacement curve from the start of the curve until the peak is achieved. The peak force represents the failure of CPB in fracture when the crack propagation begins. Since the curve does not have a simply defined equation, this value is approximated by using the available data points and calculating the area underneath each pair of points. The work of crack initiation can be therefore calculated as:

$$\text{Work} = \sum_{y=0}^{y=y_{max}} (X_{n+1} - X_n)(y_n + y_{n+1})[N * mm] \quad (3.17)$$

Where,

y_{max} = the peak force

y_n, y_{n+1} = the two force values that are adjacent

x_n, x_{n+1} = the two displacement values that are adjacent, corresponding to the force values at n

The stiffness of the sample is defined as the slope of the load-displacement curve. However, the curves developed in this testing program are not completely linear. Therefore, in order to calculate the stiffness, the linear portions of the curve are used. After examining the data, the bounds of 20% of the peak to 80% of the peak force were chosen to calculate the slope. After determining the x and y values from these points, the slope can be calculated as

$$\text{Stiffness} = \frac{y_2 - y_1}{x_2 - x_1} \left[\frac{N}{mm}\right] \quad (3.18)$$

Chapter 4 Experimental results

4.1 Effect of cement content on fracture behavior and properties of CPB

4.1.1 Effect of cement content on mode-I fracture behavior of CPB

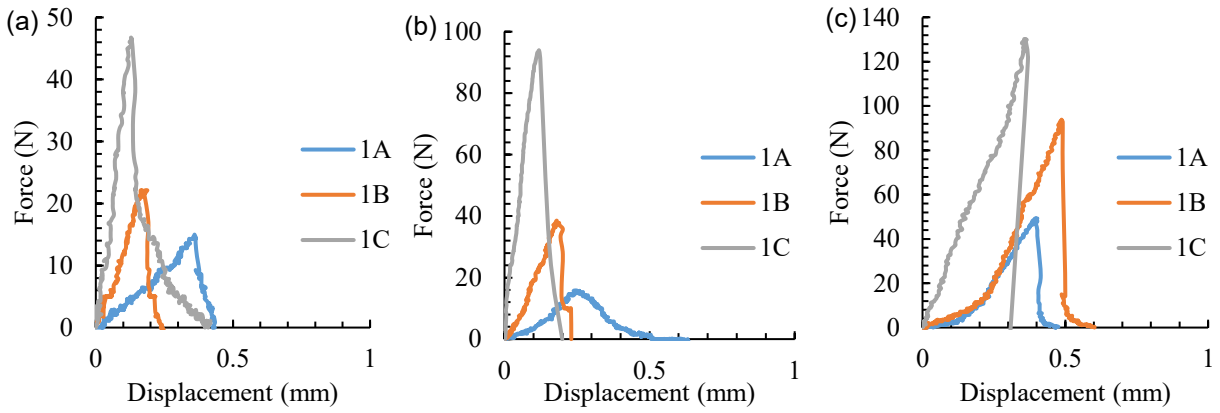

Figure 4.1: Effect of cement content on mode-I load-displacement curves of CPB at (a) 7 days, (b) 28 days, and (c) 90 days.

Figure 4.1 represents the 7-day, 28-day, and 90-day mode-I curing samples with changes in cement content. From the figure, it can be observed that the slope of the curve in the 7-day samples is much steeper with increased Cc. In addition to this, there is a post-peak behavior, which can be attributed to the sample being softer at an early age. The sample with lower Cc has a smoother post-peak behavior, unlike the 1C, which has a sudden drop before the smooth reduction in force. Of note, the post-peak drop is much steeper compared to the pre-peak, which indicates a sudden, but not total, failure. The increase in Cc represents a large improvement in the CPB peak force. Since this comparison uses only mode-I samples, the peak force can be directly correlated to the fracture toughness. The peak force at 7% Cc (Sample 1C) is more than triple that of the 2% (1A) samples. However, the increase in fracture toughness is much less when increasing from 2% to 4.5% (1B). Similar to the 7-day sample, the fracture toughness was improved with the increase in Cc in the 28- and 90-day samples. However, in the 28-day sample, the 1A and 1B curves show a significant post-peak behavior. Meanwhile, the 1C curve has a small disruption prior to the curve behaving as expected. These discrepancies are explained further in section 4.1.4. In the 90-day curves, the data shows no post-peak behavior whatsoever. The pre-peak curve shows a slow region,

which characterizes the previously mentioned adjustment period. Afterward, the force increases at a much higher rate. Once the peak is reached, a sudden drop to zero force occurs, as the sample fractures in a brittle manner. In the 90-day samples, the displacement at failure for all the differing Cc is close to 0.5mm. The 28-day samples show a lower displacement at lower cement contents, however, they have long tails which extend to the 0.5mm displacement.

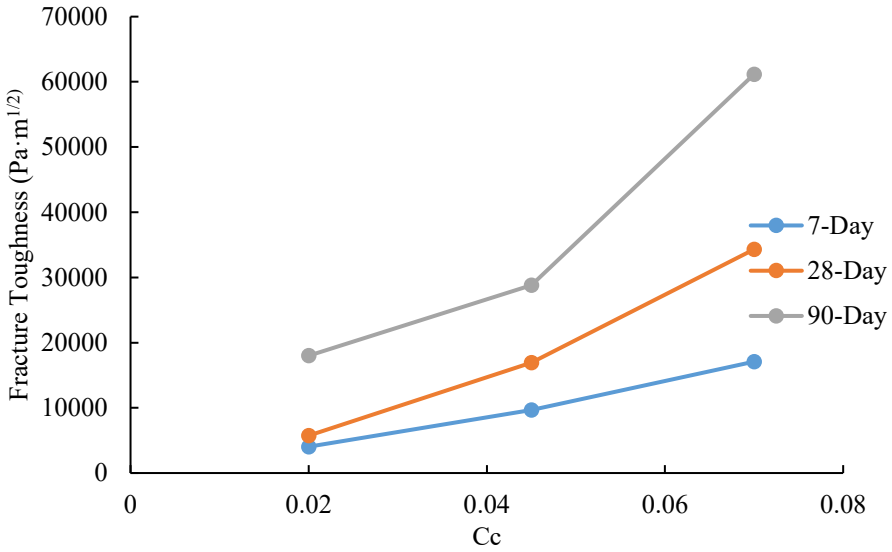

Figure 4.2: Effect of cement content on the evolutive mode-I fracture toughness of CPB.

Figure 4.2 represents the effect of cement content on the mode-I fracture toughness of CPB. At the 2% Cc, the fracture toughness is equal for 7- and 28-day samples. As the Cc increases, the curing age effect is more pronounced. There is an especially obvious effect of the Cc shown, as the 7% samples after 90 days curing time improve in strength greatly when compared to the 2%, nearly tripling in value. The effects are still pronounced in the 7- and 28-day tests. The difference between 2% Cc and 4.5% Cc is lower than 4.5% to 7%. In conclusion, the linear increase in Cc does not result in a linear improvement in fracture toughness. Another conclusion that can be drawn is that curing time is important. For example, at 7-days, the 7% Cc fracture toughness is similar to the 2% Cc at 90-days.

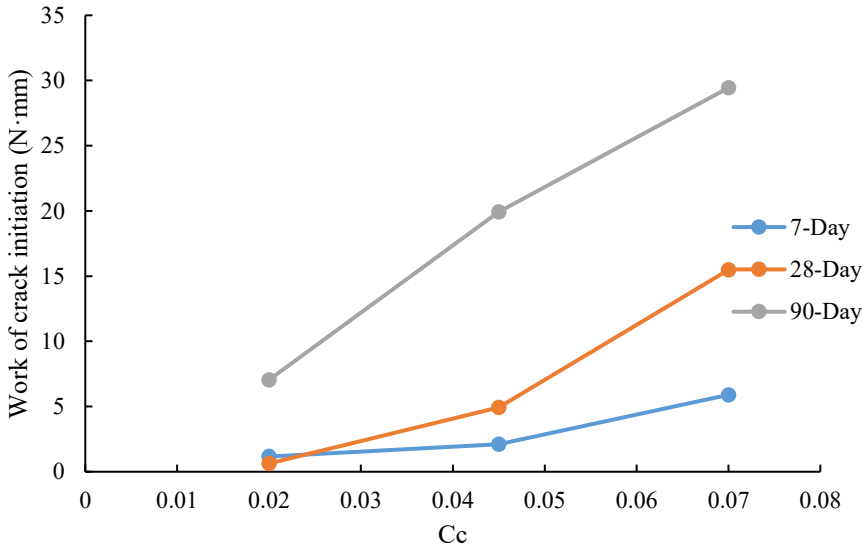

Figure 4.3: Effect of cement content on the work of crack initiation of CPB under mode-I loading.

Figure 4.3 represents the effect of cement content on the mode-I work of crack initiation in CPB The crack initiation data shows a similar trend when compared to the fracture toughness. This is expected as there is a limited post-peak behavior, and it is mostly irrelevant to the fracture toughness and crack propagation. However, in the 90-day samples, it appears that 7% Cc had a worse rate of improvement over 4.5% than the 4.5% over 2%. The work of crack initiation represents the energy input required to cause a crack to form in the sample, which accounts for the deflection in addition to the force. This explains why the 90-day curve does not have the same shape as in the fracture toughness. Since the 90-day sample experienced a high total deflection, it meant that the total energy was more spread, as opposed to focused as the force on the sample.

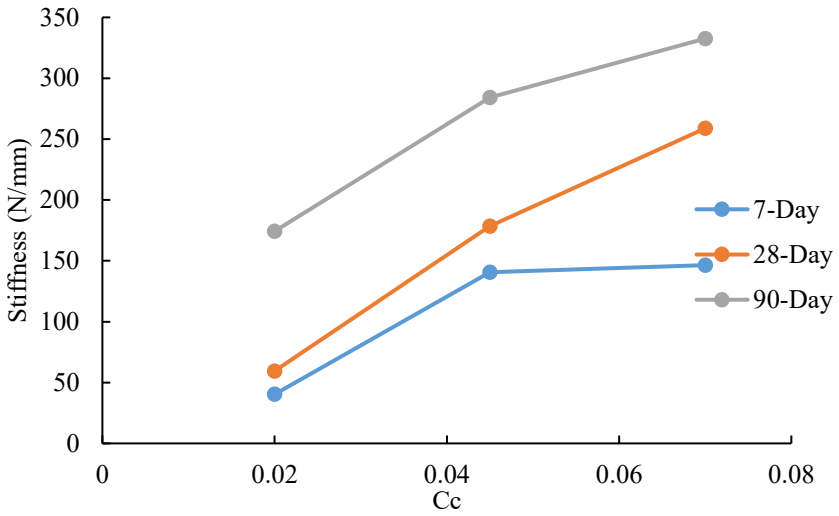

Figure 4.4: Effect of cement content on the mode-I stiffness.

Figure 4.4 represents the effect of cement content on the mode-I stiffness of CPB. In the 28-day sample, it is clear that the 7% Cc had a higher stiffness compared to the 4.5%. This is congruent with both the fracture toughness and work showing improvements with the Cc. In addition, the 7-day sample has a higher stiffness than the 28-day and 90-day samples at 7% Cc. Since the stiffness is a ratio of force to displacement, it means that the displacement had more contribution to the crack initiation compared to force. The 90-day sample shows a decreasing trend of stiffness improvement with the Cc increase, in a similar manner to work. Similarly to the fracture toughness, the stiffness at 2% Cc was similar between 7-days and 28-days.

4.1.2 Effect of cement content on mode-II fracture behavior of CPB

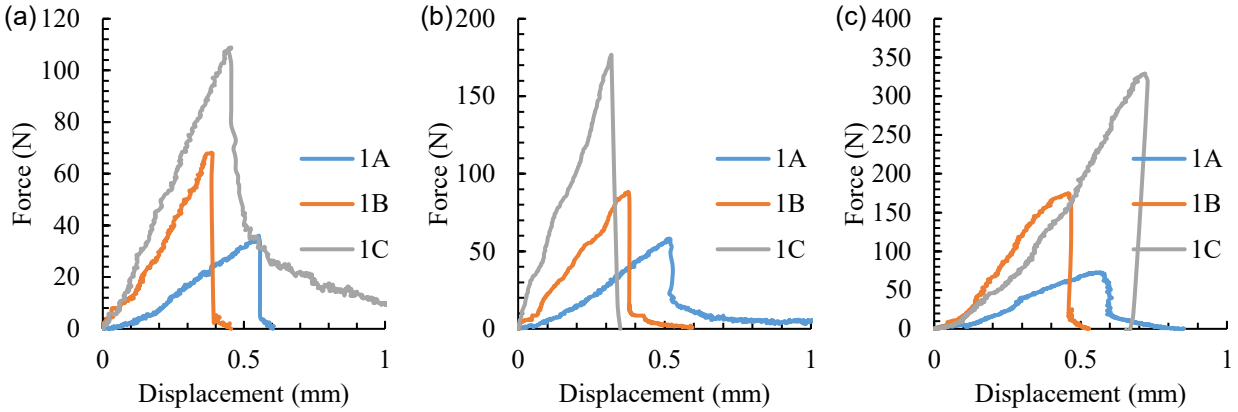

Figure 4.5: Effect of cement content on mode-II load-displacement curves of CPB at (a) 7 days, (b) 28 days, and (c) 90 days.

Figure 4.5 represents the 7-day, 28-day, and 90-day mode-II curing samples. In the seven-day samples, it can be observed that the slopes of the curves increase with the increase in Cc. The peak of the force increases with the Cc, with the 7% Cc reaching three times the peak force of the 2%. As with the mode I samples, the mode II samples peak force can be directly compared as the fracture toughness. Therefore, the fracture toughness improves by 300% from 2% to 7% Cc. In the Mode-II samples, there is almost no post-peak behavior. The peak force of the 7-day samples improves with the increase in Cc. In addition, the peaks of each sample occur at lower displacements at the higher Cc. For some of the tests, a small tail of residual force exists. This occurred when the sample had cracked, but it was not possible for the two pieces of the fractured sample to fall out of the frame after the failure. It can be seen that the actual force is very small compared to the peak. Again, in the 90-day samples, the higher Cc samples fail at a higher displacement. However, in the 28-day samples, the higher Cc resulted in failure at a lower displacement.

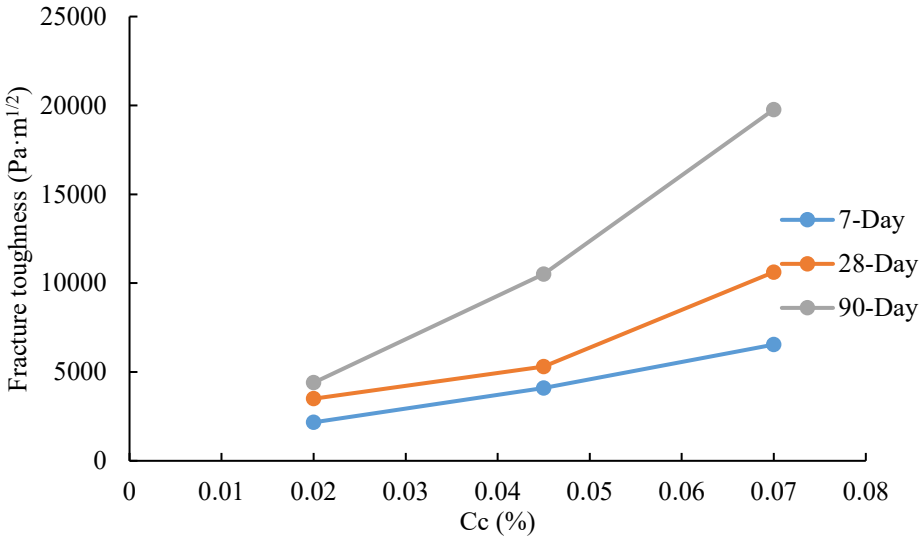

Figure 4.6: Effect of cement content on the mode-II fracture toughness.

Figure 4.6 represents the effect of cement content on the mode-II fracture toughness of CPB. As with the Mode-I samples, the 2% sample has similar fracture toughness at all ages. The mode ii fracture toughness is still affected by the curing time. However, the 2% Cc showed the least change with curing. Relative to Mode-I, the Mode-II fracture toughness is lower. Unlike the mode I samples, the mode-II 7-day and 28-day show a slow increase with Cc increase, while the 90-day shows a large improvement at 7%.

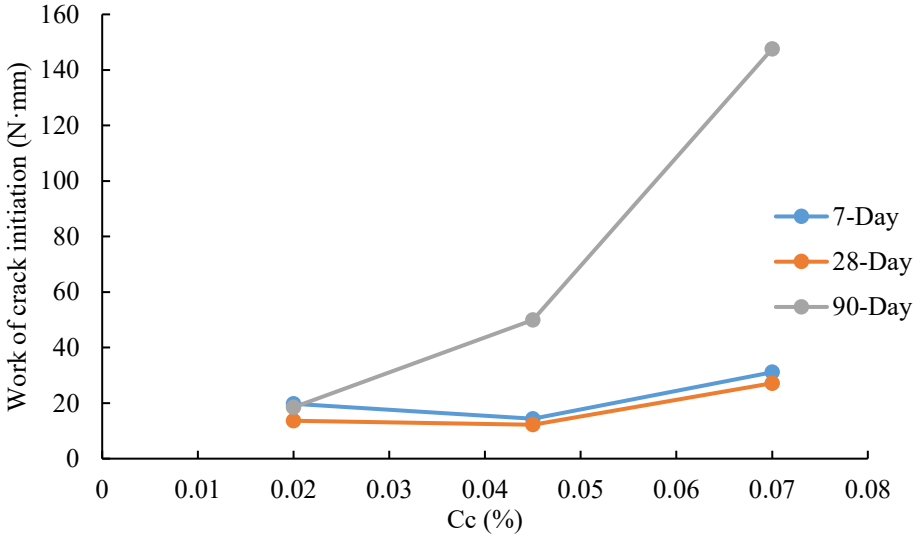

Figure 4.7: Effect of cement content on mode-II crack initiation.

Figure 4.7 represents the effect of cement content on the mode-II work of crack initiation in CPB. The Mode-II work of crack initiation for seven and 28-day samples are very similar. In addition, at the 2% Cc, the work is similar for 90-day to the other curing times. However, with the increased Cc, at 90 days the samples show a stark increase in the required work to achieve crack initiation. Although the fracture toughness is lower, the Mode-II crack initiation requires higher work compared to Mode-I failure. A major contributor to this is that the Mode-II fracture occurred at a much higher displacement.

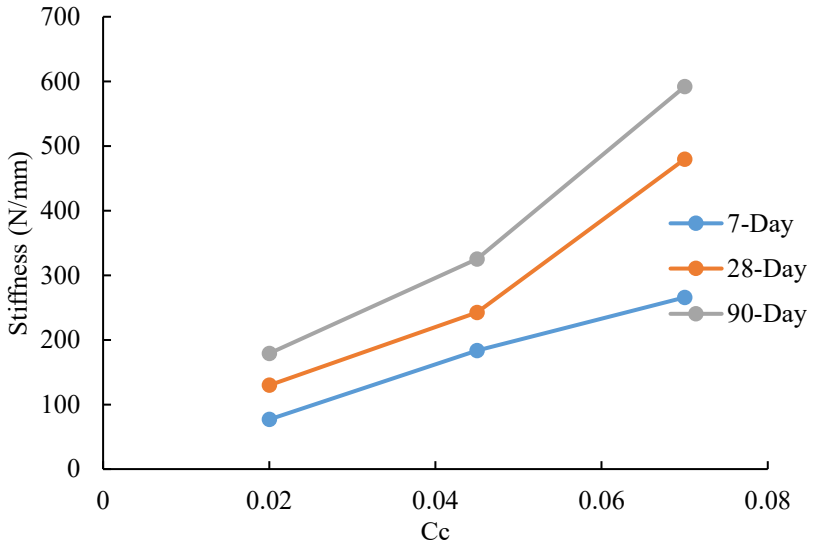

Figure 4.8: Effect of cement content on mode-II stiffness.

Figure 4.8 represents the effect of cement content on the mode-II stiffness of CPB. Overall, the stiffness of CPB increased with Cc under the Mode-II loading condition. While the 7-day stiffness increases linearly with the Cc, the 28-day saw a large improvement, and the 90-day saw some improvement over 28-day. The results in mode-II stiffness were consistent with the mode I samples. Since the mode-I and mode-II samples were obtained from the same mix, this indicates that there is an inconsistency with the calculation of the stiffness factor.

4.1.3 Effect of cement content on mode-III fracture behavior of CPB

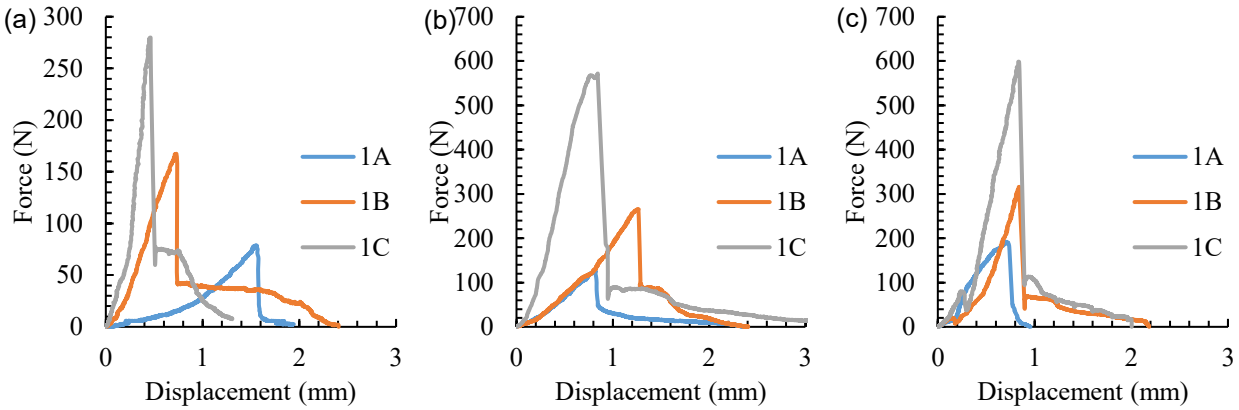

Figure 4.9: Effect of cement content on mode-III load-displacement curves of CPB at (a) 7 days, (b) 28 days, and (c) 90 days.

Figure 4.9 represents the 7-day, 28-day, and 90-day mode-III curing samples. The 7-day samples display an increase in the peak force with the increased Cc. Unlike in the previous tests, the maximum displacement can exceed 3mm, and the displacement at peak force can exceed 1mm. The Mode-III samples show the highest peak forces for all three curing periods and Cc. As the Cc increases, the slope of the load-displacement curve becomes steeper. Under the mode three fracture, the samples show a significant post-peak behavior, where the samples retain some strength after the fracture. The samples, after reaching the peak force, were observed to have a sudden crack propagation. Afterward, the crack would continue to propagate until the total collapse of the sample. The 90-day 1C sample only slightly improved in peak force when compared to 28-day. However, both nearly doubled from the 7-day sample. The 1A and 1B samples show a similar increase with the Cc as in previous modes. The 1A 7-day sample has a long build-up to the peak force. However, it has a small post-peak behavior. Meanwhile, the 28-day and 90-day 1A samples reach the peak force early. At 90-days, there is no tail. However, at 28-days, there is a significant tail. 1B is the most consistent across all three curing times.

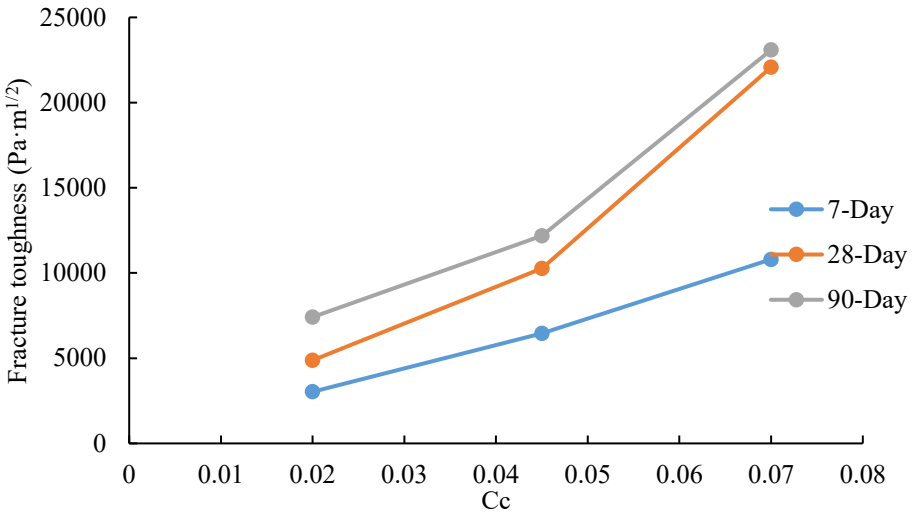

Figure 4.10: Effect of cement content on mode-III Fracture Toughness.

Figure 4.10 represents the effect of cement content on the mode-III fracture toughness of CPB. In the Mode-III, fracture toughness improves with the Cc. It appears that the Cc is a much more important factor compared to curing time in the later age samples. The mode iii samples show a linear trend in the 7-day samples. At 28-day and 90-day, a similar trend as seen in mode-I and mode II is seen, where the 7% Cc improves the fracture toughness much more than 4.5%. As mentioned before, the 28-day 7% Cc is close in fracture toughness to the 90-day 7%. The mode iii fracture toughness falls between the mode I and II samples.

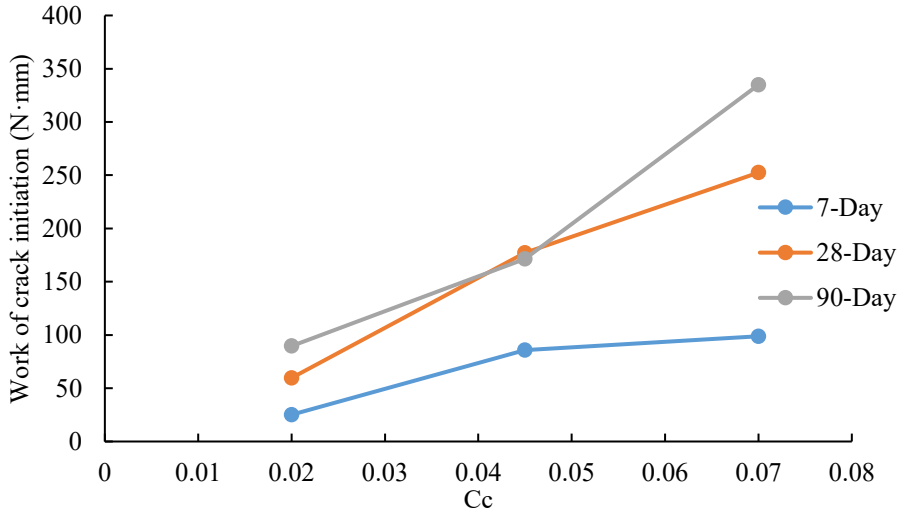

Figure 4.11: Effect of cement content on mode-III work of crack initiation.

Figure 4.11 represents the effect of cement content on the mode-III work of crack initation in CPB. The work of crack initiation in the mode-III follows a similar pattern as the mode-I and mode-II samples. While the crack initiation required the highest work for this mode, it also has the highest variance, where the 7-day Mode-III is similar to Mode-I 7-day samples. At the lower Cc, the 28-day and 90-day are very similar, while 90-day is higher at 0.07 Cc. at 7-days, the 7% Cc hardly improves the work of crack initiation over the 4.5%. Regardless, the trend is showing an improvement with the increase in Cc and increased curing time.

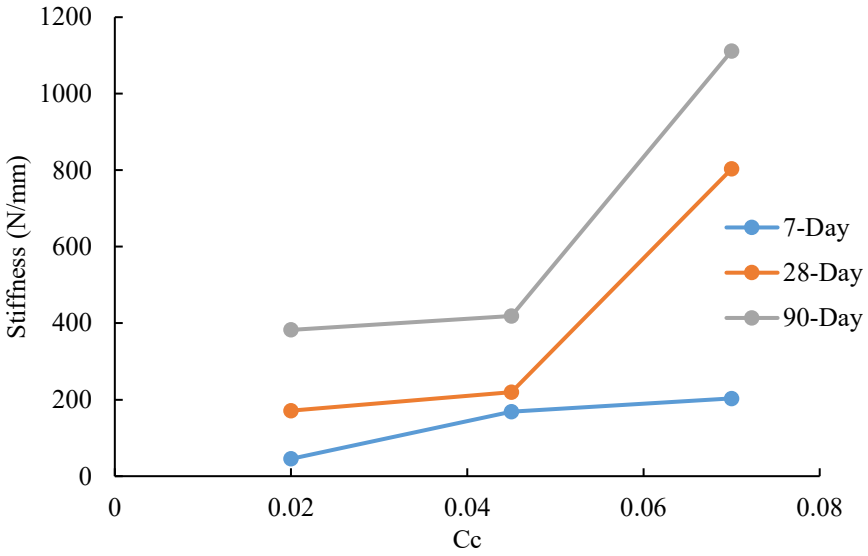

Figure 4.12: Effect of cement content on mode-III stiffness.

Figure 4.12 represents the effect of cement content on the mode-III stiffness of CPB The stiffness results show that Mode-III failure has a very high stiffness compared to other failure modes. While the 7-day shows a linear progression, the 28-day and 90-day improved more with the higher Cc. Of note, the 28-day stiffness is higher than 90-days at 7% Cc. However, at 4.5%, the 28-day sample has the lowest stiffness. Overall, the 7% Cc has the highest stiffness for each curing period.

4.1.4 Effect of cement content on fracture properties of CPB

Examining the porosity and saturation data for the mode-I samples, there is a trend of reduced porosity while increasing the degree of saturation as the Cc increases. The porosity results seem to confirm the effects of increased Cc improvements on fracture toughness. As seen in the previous studies, an increase in the Cc leads to a reduction in the pore size and spacing, thereby improving

the CPB strength. However, the saturation results appear to indicate the increase of saturation with Cc. This is contradictory to expected results, as the increased Cc should result in the increased consumption of water to form hydration products. However, one of the three tests is not consistent with the other two, and in addition, they are not consistent with the later-stage results. This suggests that it could be a result of the early age cuing, where the hydration process is still ongoing, and therefore some inconsistent saturation results occurred. Finally, the GWC does decrease with the increase in Cc, showing that the hydration process is proceeding as expected.

These discrepancies can be attributed to the method of testing. While careful consideration was put into ensuring the accurate positioning of the samples in the loading frame, there could be several concerns. For example, when the sample is loaded, the frame must be adjusted, so the sample touches the three bars. This is done by moving the base platform vertically until the top of the sample makes contact with the bottom of the loading bar. In addition, while a laser level was used to ensure the top of the sample was in contact with the bottom of the bar, the sample could be off by a few millimeters. This could be the result of slight misplacing of the sample, or of a slightly loose loading bar. If it is slightly loose, an adjustment period can be observed. To account for this, the calculation of stiffness is performed between the ranges of 20% and 80% of the curve, or up to the peak. Taking this into consideration, the stiffness of the 1B sample is slightly higher than 1C. The porosity and degree of saturation for both 28 and 90-day samples show a decreasing trend as the Cc increases. Another trend noted in the Mode-I samples is that the 1C samples have a lower stiffness compared to the 1B. It is possible that the later ages have less effect on the stiffness in Mode-I compared to modes II or III. As the Cc increased in Mode-II samples, the fracture toughness increased significantly. As with the other samples, a 7-day 7% Cc sample exceeds the toughness of a 90-day 2% Cc sample. Since this mode represents the in-plane shear of CPB, it shows the importance of fracture behavior to the design of CPB stopes. In the Mode-III samples, the trend of Cc improving the fracture toughness is confirmed again. The slopes also trend higher with the increased Cc, indicating a higher stiffness.

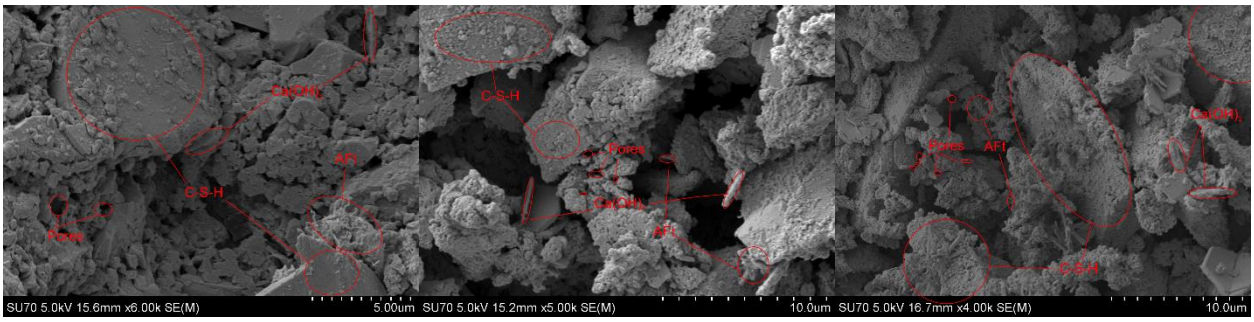

(A) (B) (C)

Figure 4.13: SEM images of 7-day CPB with different cement content (A) 2%, (B) 4.5%, and (C) 7%.

As seen in the SEM results for the 7-day samples (Figure 4.13), with the increase of Cc, the size of the pores decrease, which indicates an improvement in the self-desiccation effect. The increase also provides larger C-S-H volumes, which binds the CPB together. There is a significant amount of AFt (ettringite) in all of the samples. The calcium hydroxide crystals are small and scattered randomly.

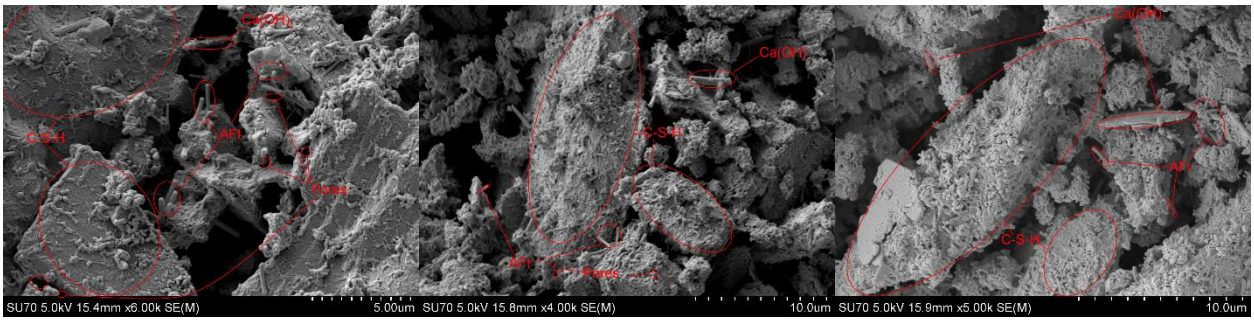

(A) (B) (C)

Figure 4.14: SEM images of 28-day CPB with different cement content (A) 2%, (B) 4.5%, and (C) 7%.

Figure 4.14 shows the SEM comparison of Cc effect on 28-day samples. Compared to the 7-day samples, the 28-day samples show larger C-S-H sections. The pores are also smaller and more uniformly distributed. There is less free AFt compared to 7-day samples, instead sticking to the C-S-H in large clusters. The C-S-H surrounds the Aft, and thus the AFt acts as a connection between C-S-H clusters. Looking at the Cc increase, it is clear that higher Cc leads to larger C-S-H crystals and smaller, more uniform pores.

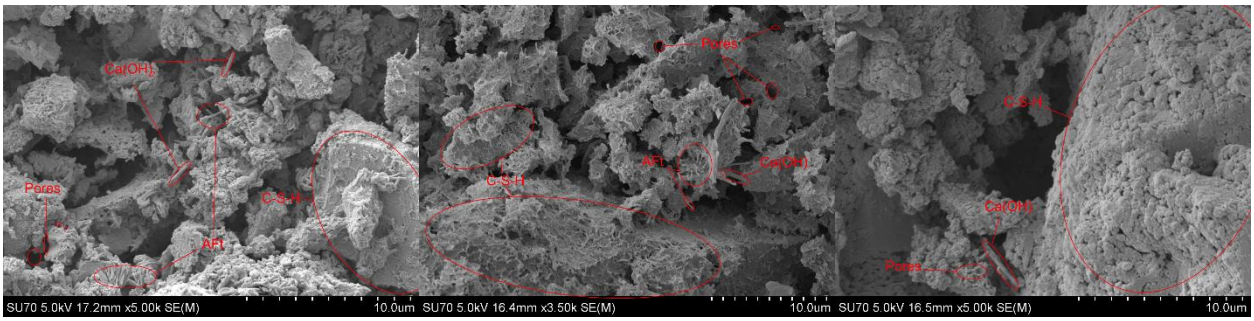

(A) (B) (C)

Figure 4.15: SEM images of 90-day CPB with different cement content (A) 2%, (B) 4.5%, and (C) 7%.

Figure 4.15 shows the effect of Cc on the 90-day sample's microstructure. In the 90-day samples, the C-S-H takes up the majority of the CPB microstructure. Meanwhile, there is very little of the AFt and $Ca(OH)_2$. On the tops of C-S-H clusters, a significant amount of small AFt crystals can be seen. The pores are even smaller compared to the earlier age samples, and the pores are evenly distributed within the C-S-H. In the 90-day sample, a single C-S-H cluster takes up half of the viewport of the SEM. Meanwhile, there is almost no visible ettringite. The difference in the volume of C-S-H clusters between the 2% and 7% samples is most visible at this point.

4.2 Effect of hydraulic factors on fracture behavior and properties of CPB

4.2.1 Effect of hydraulic factors on mode-I fracture behavior of CPB

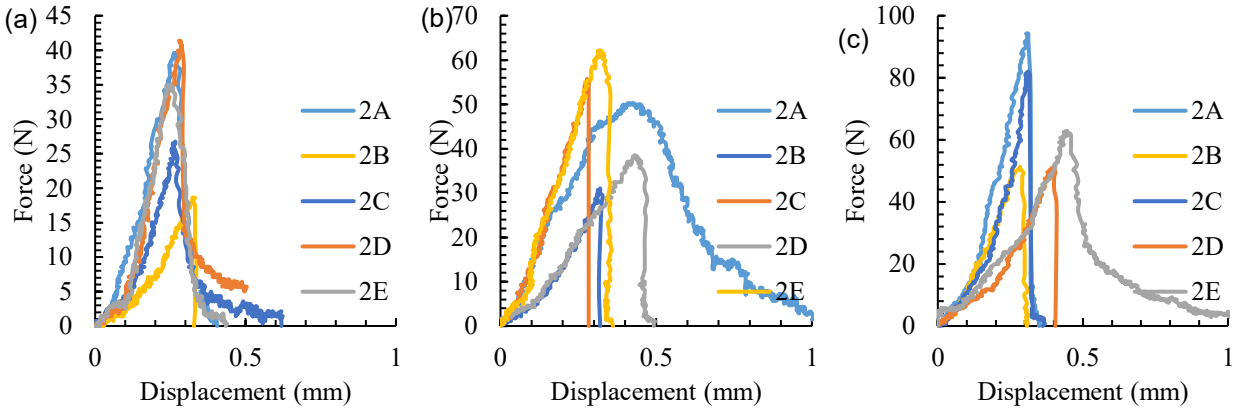

Figure 4.16: Effect of hydraulic factors on mode-I load-displacement curves of CPB at (a) 7 days, (b) 28 days, and (c) 90 days.

In Figure 4.16, the 7, 28, and 90-day CPB Mode-I samples are shown, displaying the samples with altered hydraulic factors. Set 2A represents the 0.33 WTR. Meanwhile, 2B is the 0.39 WTR. Sets 2C, 2D, and 2E all represent the same mix design as sample 1B, but under unique curing conditions, as mentioned in the methodology. The key takeaway is that the reduced water content reveals an improvement in the peak force. The 0.36 WTR, drained condition and resaturated conditions all result in similar peak force and slope. It is possible that the resaturation has no effect on the Mode-I early age strength. Overall, the water content has a minimal effect on the slope of the curves. For the 7-day samples, the post-peak is almost an instant drop.

In the 28-day samples, the 2E set has the highest peak force. Meanwhile, it was quite low at 90 days. The effect of removing moisture after curing appears to be inconsistent. It could be that, due to the method of oven drying, the results were inconsistent. However, it was clear that at the late stages of curing, the resaturation weakened the CPB.

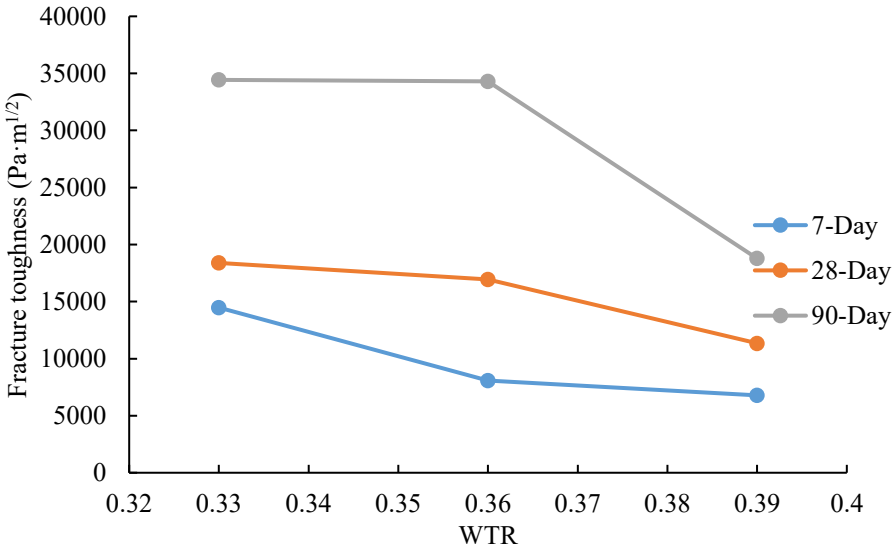

Figure 4.17: Effect of initial water content (WTR) on mode-I fracture toughness.

In Figure 4.17, the effect of changing the WTR on the fracture toughness in mode-I samples is shown. With the increase in the WTR, the samples showed a lower fracture toughness. While this is the case, reducing the WTR was not very effective at improving the fracture toughness in Mode-I. Overall, the most prominent effect shows in the 90-day sample, where the 0.39 WTR resulted in a massive drop in fracture toughness. However, the 0.33 fracture toughness is only slightly

improved when compared to 0.36. Compared to the effects of Cc improvement, the mode I fracture toughness was improved significantly more by using 7% Cc, as opposed to reducing WTR to 0.33.

Another measure of the effect of water content is the use of GWC. By comparing the measured GWC with fracture toughness, the effect of different in-situ conditions, such as water drainage, can be observed. At the lowest GWC, the samples show a high fracture toughness, then reduce before gaining strength again. With the exception of the 90-day samples, they do not achieve the maximum fracture toughness that is at the lowest water content. The 28-day sample progresses as expected. However, with only a slight increase in GWC, there is a steep drop in fracture toughness.

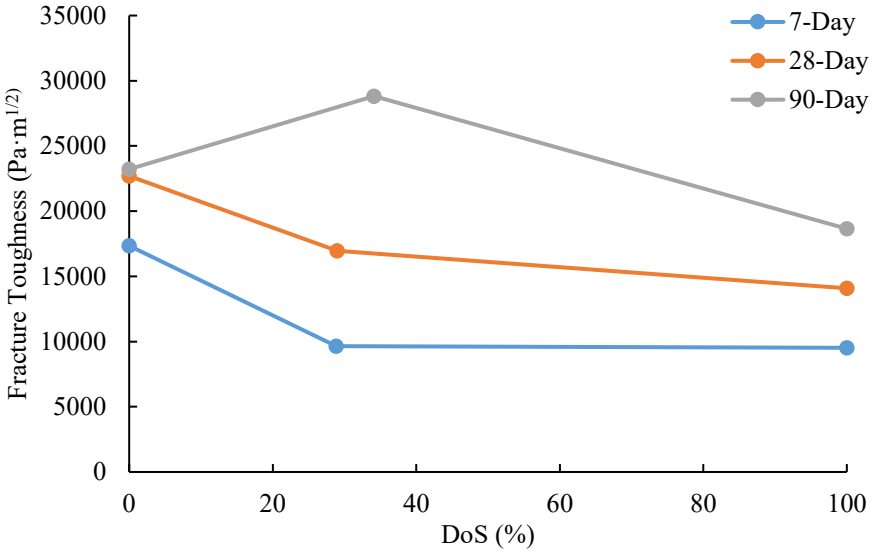

Figure 4.18 Effect of DoS on mode-I fracture toughness.

In Figure 4.18, a comparison of fracture toughness and the degree of saturation (DoS) is shown. There is a negative correlation between the DoS and the fracture toughness, although in the 90-day sample, a significant increase in the toughness can be observed at a higher DoS before it drops again. The fracture toughness may have dropped due to the drying process at 90 days. Since the 90-day sample had more time to cure, the drying process had the potential to cause microcracking. At the lower curing ages, there was still significant hydration occurring, so the drying process did cause some microcracking. However, the matric suction force resulted in a net positive. Meanwhile, the resaturation had minimal effect, as there was remaining hydration.

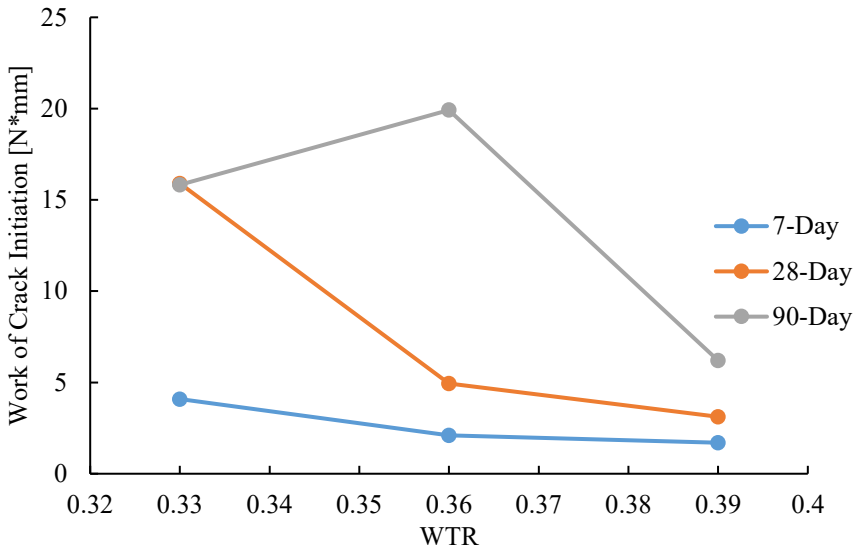

Figure 4.19: Effect of WTR on mode-I work of crack initiation.

In Figure 4.19, the effect of WTR on work of crack initiation is shown. When looking at the crack initiation, the 7-day and 28-day samples require less work to begin crack propagation when the WTR increases. The 90-day sample shows an increase in the 0.36 WTR range. At the 90-day aging, the 0.36 WTR appears to be beneficial to crack initiation. At an early age, however, it is more beneficial to have low WTR. The results from WTR effect on work are similar to those of the DoS on fracture toughness. At 90-days, the 7% Cc was more effective at improving work of crack initiation (i.e., increasing work required to form crack) when compared to reducing WTR. Therefore, Cc increase is more effective at improving CPB when compared to altering WTR.

As the GWC decreases, the Mode-I sample experiences a decrease in the work of crack initiation. In the 7-day and 28-day samples, the slope of the data becomes steeper as the GWC approaches 0.32. However, at 0.31 WTR, the 7-day sample has a slight increase in the work. This could be a result of the sample becoming softer and therefore failing at a higher displacement. The 90-day sample had a similar work of crack initiation as the 28-day sample, even though the 28-day sample has a higher GWC. However, the 90-day sample stays at a lower GWC for all samples, and maintains a higher work.

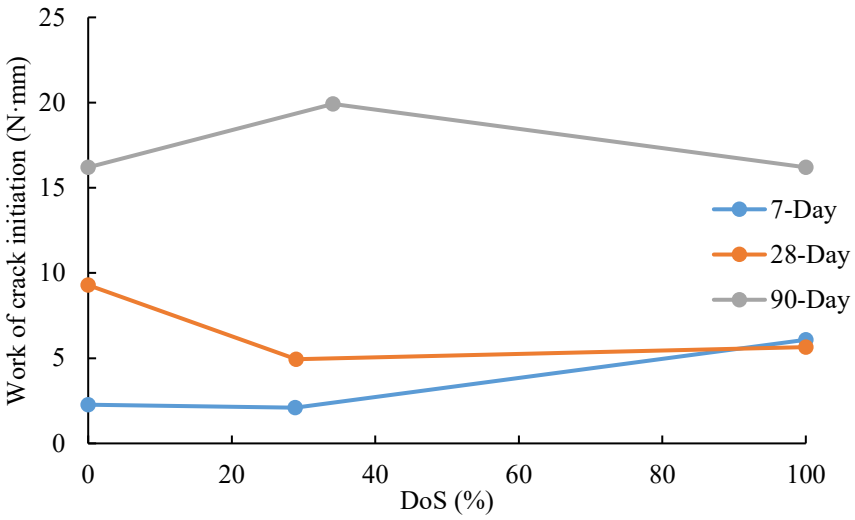

Figure 4.20: Effect of DoS on mode-I work of crack initiation.

Figgure 4.20 shows the effect of DoS on the work of crack initation in mode-I. With regards to the DoS, the samples at seven days and 28 days show an initial decrease before increasing the work of crack at 100%. Meanwhile, the 90-day sample shows an inverse pattern. The cause of this could be that due to the extra saturation, the sample becomes softer, which results in a longer displacement at 90 days, and, thereby, a lower peak force. Meanwhile, the less aged samples were already softer due to less water reaction. Overall, the 90-day sample still requires much higher energy to reach fracture.

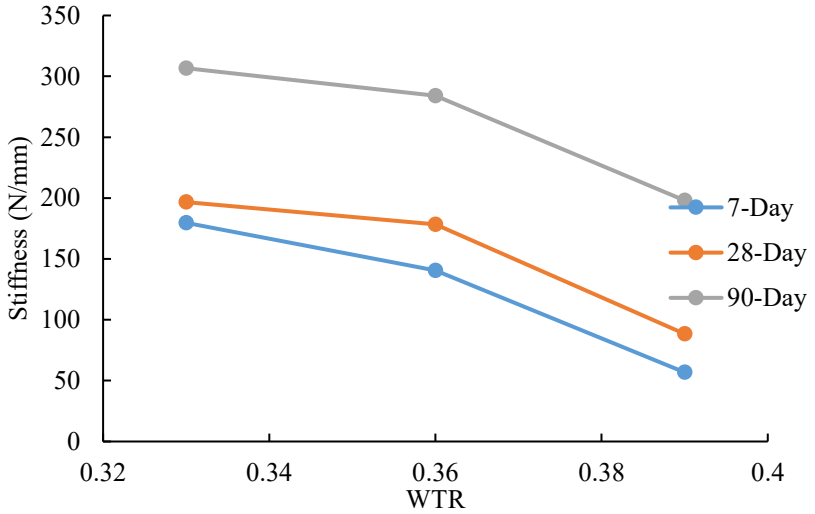

Figure 4.21: Effect of WTR on mode-I stiffness.

Figure 4.21 displays the effect of WTR on the mode-I stiffness. As the initial water content increases, the samples show a decrease in stiffness. This is likely due to the higher water content leaving more residual water, which results in lower matric suction. The 28-day stiffness at 0.33 WTR is lower stiffness than the 7-day. The 28-day sample shows a peak at 0.36 WTR. Meanwhile, the 28-day sample at 0.33 WTR has a lower stiffness than the 7-day sample. The 90-day stiffness is dominant at all WTR. For all three curing periods, the 0.39 WTR is the lowest stiffness.

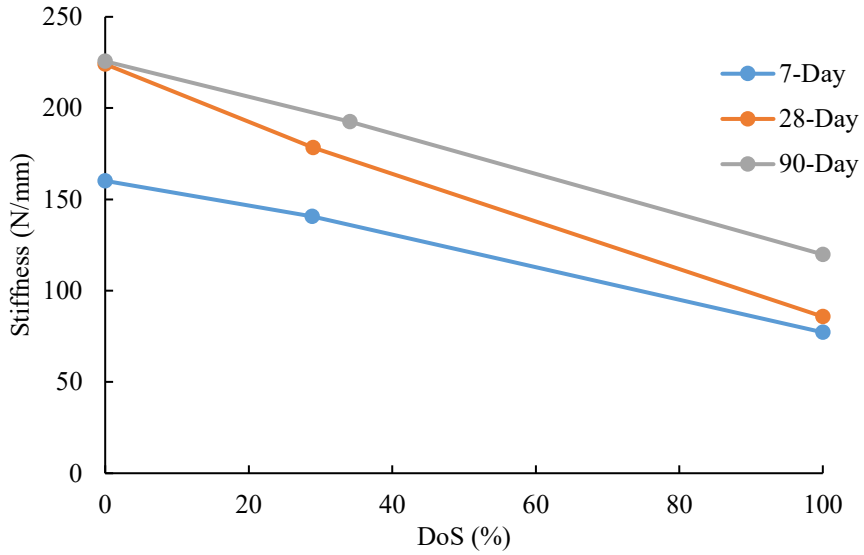

Figure 4.22: Effect of DoS on mode-I stiffness.

Figure 4.22 displays the effect of DoS on the mode-I stiffness. The stiffness observed in the samples follows a similar pattern to the fracture toughness. However, at the earlier stages of hydration, this intermediate saturation is weaker. The 7-day sample shows the maximum stiffness at 100% saturation, and minimum at 28.9%. the 28-day sample decreases linearly with the increasing DoS.

4.2.2 Effect of hydraulic factor on mode-II fracture behavior of CPB

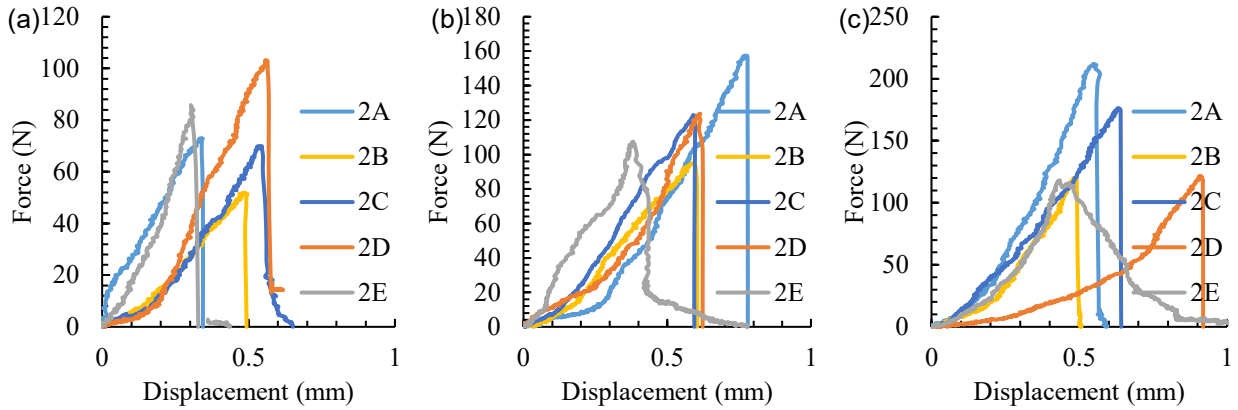

Figure 4.23: Effect of Hydraulic Factors on mode-II load-displacement curves of CPB at (a) 7 days, (b) 28 days, and (c) 90 days.

In Figure 4.23, the 7, 28, and 90-day CPB Mode-II samples are shown, displaying the samples with altered hydraulic factors. In the Mode-II samples, the 2D samples showed the peak force in the 7-day samples. As the curing age increases, the 2D samples are relatively weaker than the others. In the 28 and 90-day, the 2A samples achieve the highest peak force. It appears, however, that the peak force is not massively increased when the water content is reduced. Meanwhile, the increased water content is sometimes very damaging to the samples. The 2E samples also show an abnormal curvature. This could be a result of microcracking due to the sudden drying process. Unlike the Mode-I samples, there is a variance in the peak displacement. However, most of the samples fall around the 0.5mm displacement. The slope of the curves is relatively similar. However, some of the curves are bimodal; they experience a shallow slope before adopting a much deeper one. None of the seven-day samples show any form of post-peak behavior. Only the dried samples in 28 and 90-day samples show any post-peak behavior.

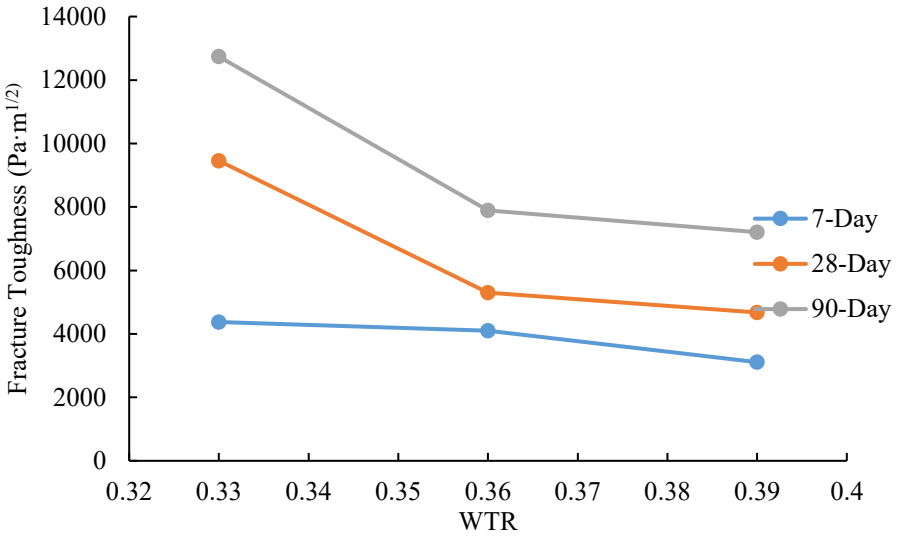

Figure 4.24: Effect of WTR on mode-II fracture toughness.

Figure 4.24 shows the effect of WTR on the mode-II fracture toughness. As with the Mode-I samples, the increase in WTR decreases the fracture toughness. The 90-day samples are a stronger lower water content. While this is the case, reducing the WTR was not very effective at improving the fracture toughness in Mode-II. Rather, increasing the WTR ratio only served to damage the fracture toughness. Therefore, it appears that reducing WTR past 0.36 is not very effective at improving fracture properties. The effect is much less pronounced in the 7-day samples.

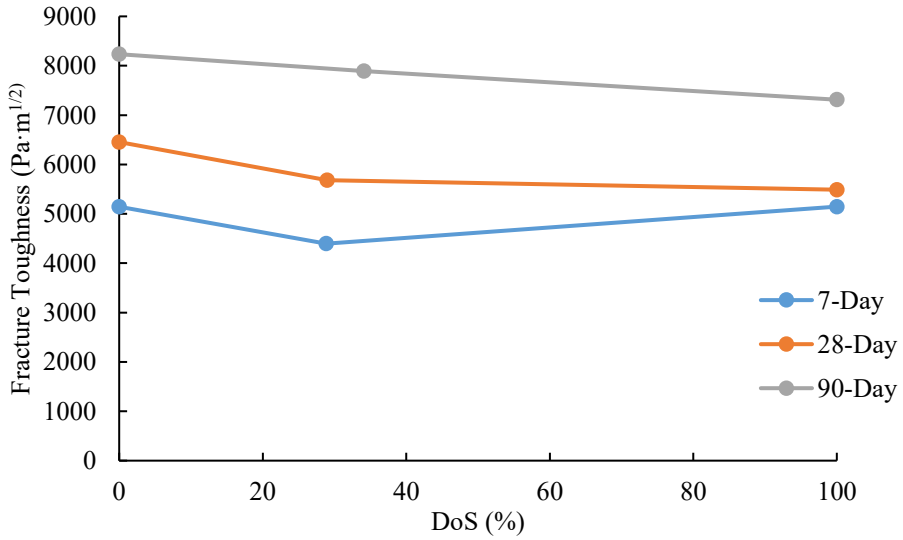

Figure 4.25: Effect of DoS on mode-II fracture toughness.

Figure 4.25 shows the effect of DoS on the mode-II fracture toughness In the Mode-II samples, the force once again peaks in the 90-day samples. Again, this peak occurs at the intermediate DoS of 34.1%. Meanwhile, for the lower curing times, the samples show a weaker point at the middle saturation. The 90-day and 28-day samples are very close at 100% saturation, and all three samples show a similar fracture toughness at 0% saturation. It is clear that the fully saturated and fully unsaturated conditions are less ideal for CPB strength at higher ages. Meanwhile, at an early age periods, the drying or resaturation provided an improved fracture toughness. To achieve a higher early age strength, one of these techniques may be ideal.

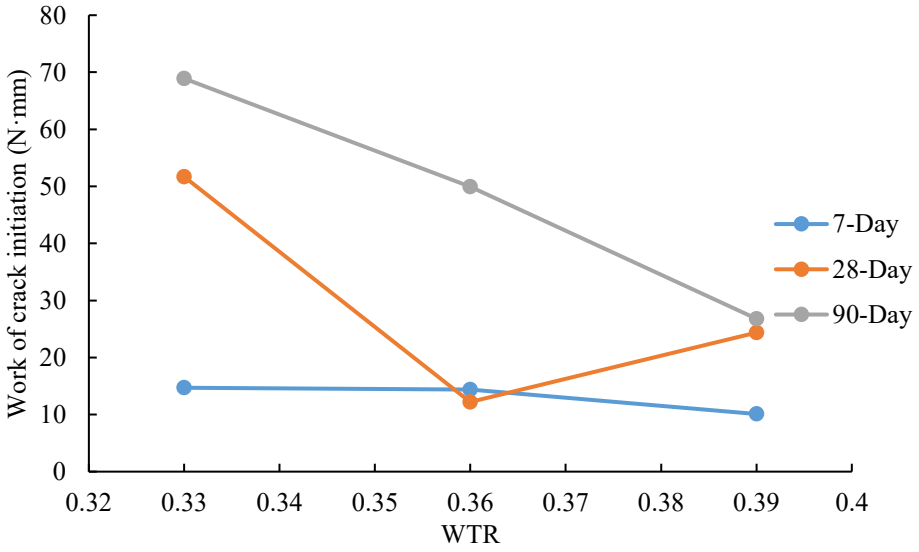

Figure 4.26: Effect of WTR on mode-II work of crack initiation.

Figure 4.26 shows the effect of WTR on the mode-II work of crack initiation. The 7-day and 28-day samples require less work to begin crack propagation when the WTR increases. The 90-day sample shows a downwards trend for crack initiation. At the 90-day aging, the 0.33 WTR requires the most work to initiate cracking. At an early age, the WTR has minimal effect on Mode-II samples. At an early age, it is beneficial to have low WTR. The results from WTR effect on work are similar to those of the DoS on fracture toughness. The work of crack initiation for mode-II samples is much higher compared to mode-I.

As with the Mode-I samples, the 90-day Mode-II samples decrease in work required as the GWC

increases. There is an increase in the work at the higher GWC. Around the 0.31 GWC, there is a sudden increase in the work required. The 90-day sample has consistently higher work at similar work to the other curing periods. The 7-day samples experience almost no change in work regardless of the GWC. the 28-day sample shows the most sudden change, with the 0.31 GWC reducing and then increasing to match the work of 0.306 GWC.

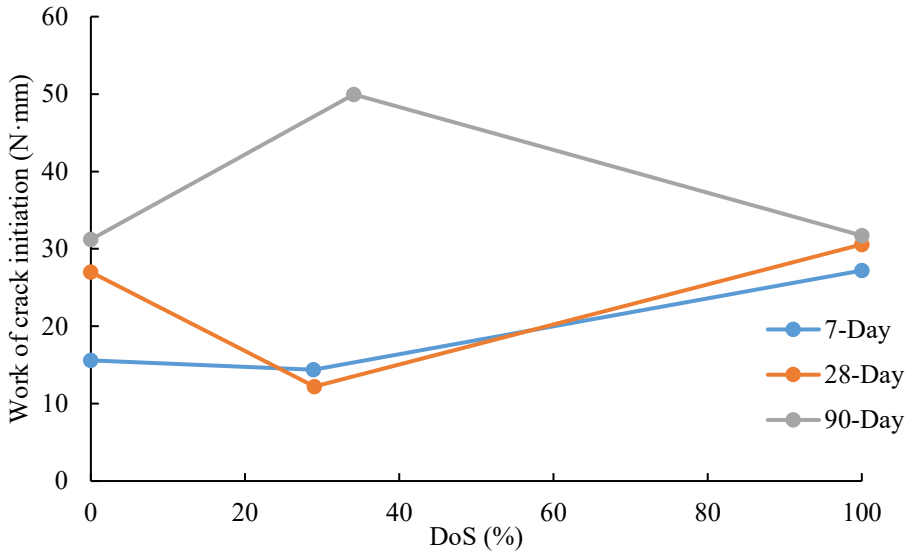

Figure 4.27: Effect of the DoS on mode-II work of crack initiation.

Figure 4.27 shows the effect of DoS on the mode-II work of crack initiation. Similar to the samples in Mode-I, the 90-day sample's work peaks at 34.1% saturation, meanwhile it reaches a minimum for the 7-day and 28-day samples. The change in saturation state had negative effects on the work required for the 90-day sample. Overall, the 90-day sample still requires much higher energy to reach fracture at all saturation states. However, the work required at 90-days and 28-days for the 100% and 0% DoS is very similar.

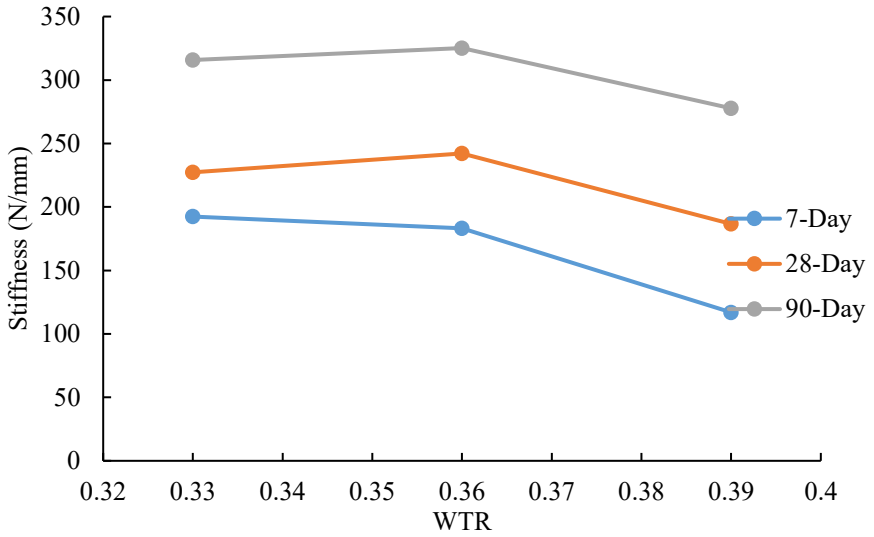

Figure 4.28: Effect of WTR on mode-II stiffness.

Figure 4.28 shows the effect of WTR on the mode-II stiffness. The Mode-II samples show that the 0.33 WTR has the highest stiffness. The stiffness is almost identical for 0.33 WTR and 0.36 WTR. The 7-day and 28-day sample's stiffness is barely affected by changes in the WTR. Overall, the curing period shows the expected effect of improving stiffness. Compared to mode-I, the stiffness is much higher in mode-II samples. However, the effect of WTR on the stiffness of Mode-II samples does not follow the same pattern.

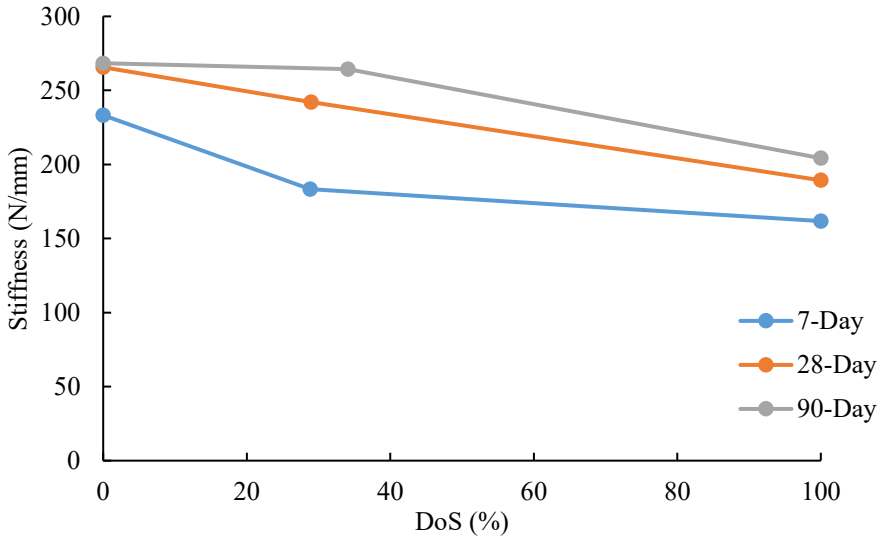

Figure 4.29: Effect of DoS on Mode-II Stiffness.

Figure 4.29 shows the effect of DoS on the mode-II work of crack initiation. As shown in the Mode-I sample, the 90-day sample stiffness peaks at the 28.9% DoS. Meanwhile, the 7-day and 28-day samples show a minimum of 28.9%. The 7-day and 28-day samples are almost identical in terms of stiffness, regardless of the DoS. The 28-day performs slightly worse at full saturation and unsaturated. However, it is better at the intermediate saturation. Unlike the mode-I, there is no clear trend in any of the curing periods to determine the effects of DoS on mode-II stiffness.

4.2.3 Effect of hydraulic factor on mode-III fracture behavior of CPB

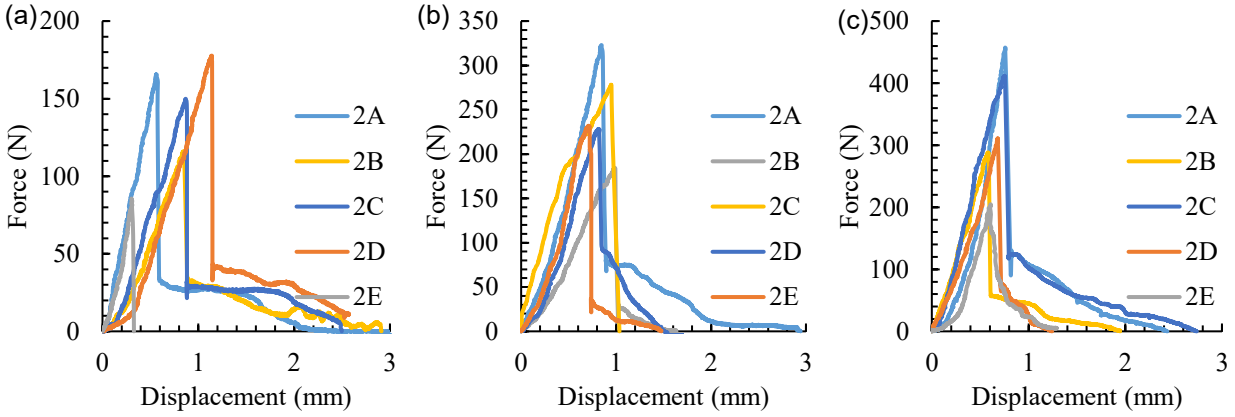

Figure 4.30: Effect of hydraulic factors on mode-III load-displacement curves of CPB at (a) 7 days, (b) 28 days, and (c) 90 days.

In Figure 4.30, the 7, 28, and 90-day CPB Mode-III samples are shown, displaying the samples with altered hydraulic factors. In the Mode-III, it is shown that a significant post-peak behavior occurs. Again, in the early age samples, the resaturated sample is the highest peak force. However, it diminishes at the higher curing ages. The unsaturated sample shows a low strength in all curing periods. At the 28 and 90-day curing, the 2A sample is the highest peak force. The drained sample, meanwhile, nearly matches with 2A. Almost all of the samples reach their peak force at 0.5mm, with the exception of the 7-day samples. The majority of samples at 7-day reach a similar peak force of around 175 N. The 28-day samples, meanwhile, mostly reach a force around 275 N.

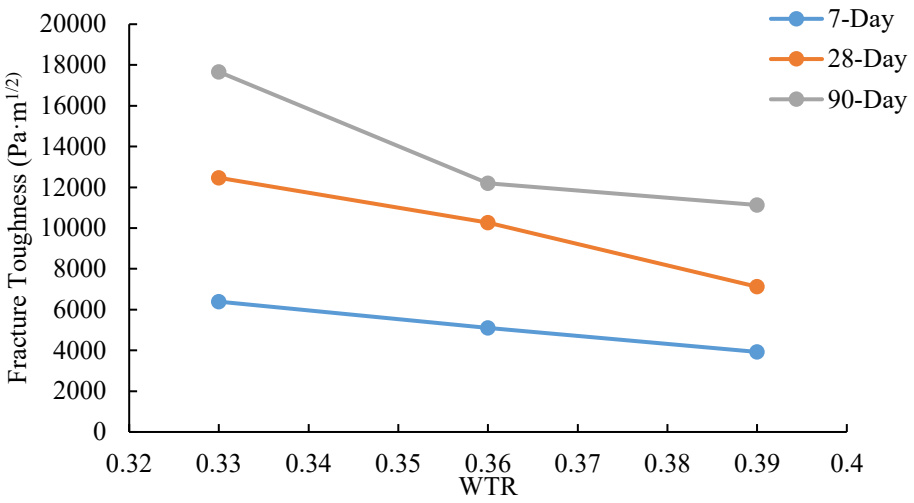

Figure 4.31: Effect of WTR on mode-III fracture toughness.

In Figure 4.31, it is shown that with the increase in the WTR, the samples showed a lower fracture toughness. While this is the case, reducing the WTR was somewhat effective at improving the fracture toughness. Overall, the most prominent effect shows in the 90-day sample, which maintains the highest fracture toughness at all WTR. At 0.39 WTR, the 7-day sample increases and the 28-day decrease to reach a similar fracture toughness. At lower WTR, the 28-day samples have a higher fracture toughness. The 7-day samples actually decrease in fracture toughness as the WTR decrease. The mode-III fracture toughness at 0.33 WTR surpasses the 4.5% Cc. However, it is worse than 7% Cc.

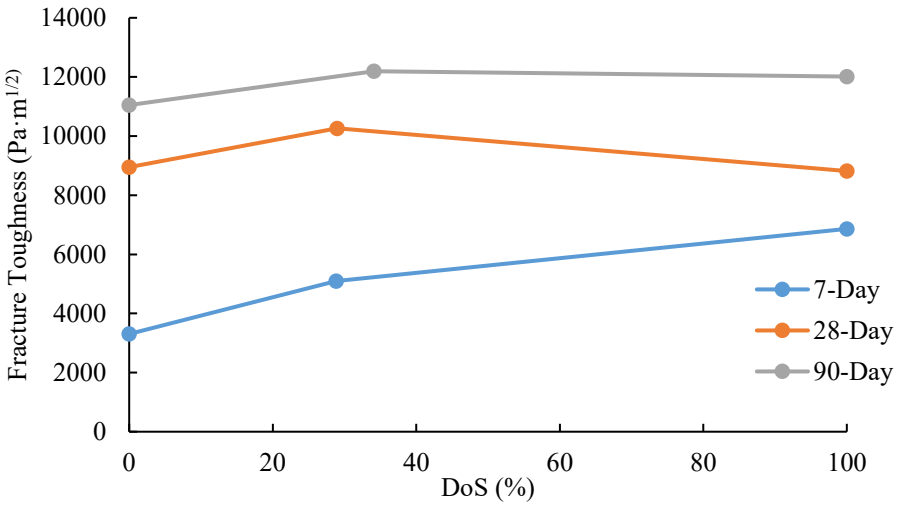

Figure 4.32: Effect of DoS on mode-III fracture toughness.

Figure 4.32 shows the effect of DoS on the mode-III fracture toughness. In this figure, a comparison of fracture toughness and the degree of saturation (DoS) can be made. At the 30% DoS, the fracture toughness increases before decreasing at 100% for the 28-day and 90-day curing periods. In the unsaturated condition, the 90-day sample has a lower fracture toughness than the 28-day sample. However, it performs better at higher DoS. The 7-day period shows an increase with the increased DoS. It appears that the drying process to desaturate the samples caused a significant reduction in fracture toughness. Overall, the unsaturated samples appear to perform worse than expected with regard to fracture toughness. When compared to the other modes, Mode-III samples showed an intermediate fracture toughness.

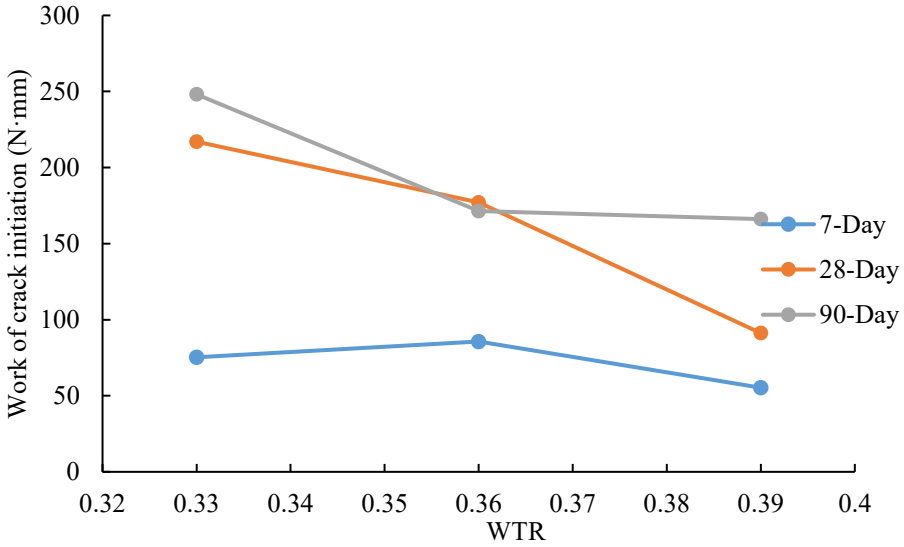

Figure 4.33: Effect of WTR on mode-III work of crack initiation.

Figure 4.33 shows the effect of WTR on the mode-II34I work of crack initiation The 0.36 WTR at 7 days provides the highest Work of Crack Initiation. However, at the higher curing times, the 0.33 WTR has the highest work, while they are equivalent at 0.36. At the lower WTR, the 90-day sample has the highest work required to achieve crack initiation. However, the 28-day sample is close. The 7-day sample requires a very low amount of work to crack, comparatively. The Mode-III samples had a higher work of crack initiation when compared to the equivalent mode-I and mode-II samples.

As the GWC decreases, the samples experience a decrease in the work of crack initiation. In the 7-day and 28-day samples, the slope of the data becomes steeper as the GWC approaches 0.32. The 90-day sample shows an erratic pattern, first decreasing, then increasing, before decreasing again. The peak appears around 0.295 GWC. Meanwhile, the 28-day sample decreases with the increase in GWC. Finally, the 7-day shows a decreasing trend before increasing after 0.31 GWC. The mode-III samples have the most inconsistent results for stiffness compared to GWC.

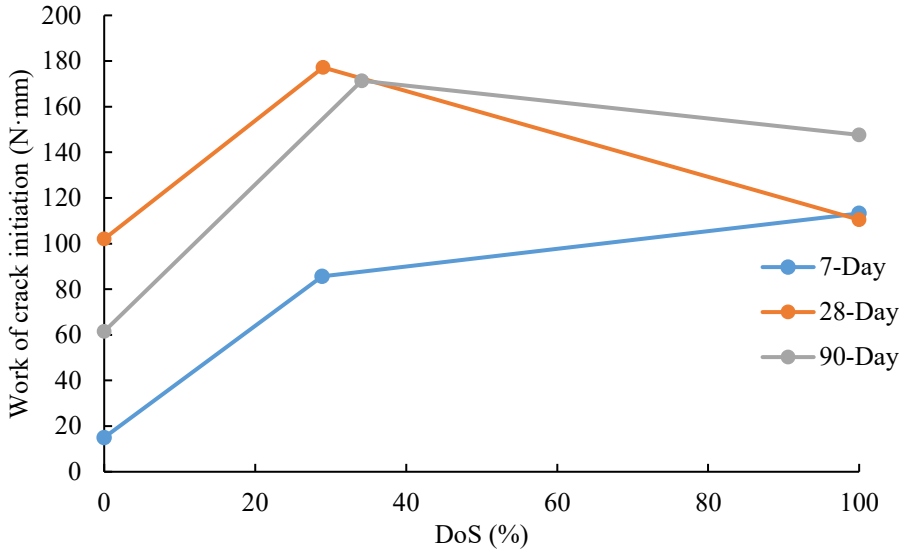

Figure 4.34: Effect of DoS on mode-III work of crack initiation.

Figure 4.34 shows the effect of DoS on the mode-III work of crack initiation With regards to the DoS, the samples at 7-days, 28-days, and 90-days show an initial increase before decreasing in the work of crack at 100%. Overall, the 90-day sample has a similar work of crack initiation to 28-day at the intermediate DoS. However, the 28-day sample has a higher peak work. Meanwhile, the 7-day curing period shows an increasing trend with the increase in DoS. The 28-day and 7-day work are equivalent in the fully saturated state, whereas the 90-day sample has a higher work of crack initiation.

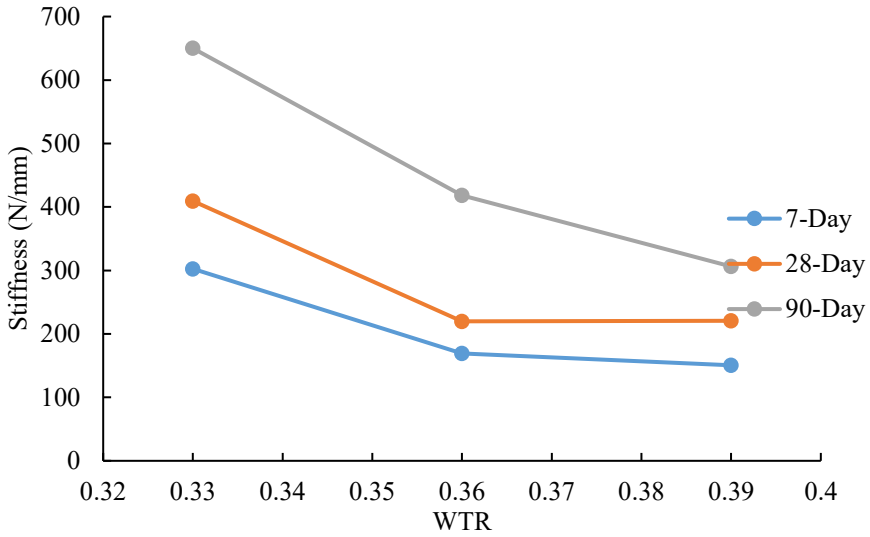

Figure 4.35: Effect of WTR on mode-III stiffness.

Figure 4.35 shows the effect of DoS on the mode-III stiffness. At 0.36 WTR, the sample stiffness at 90 and 28 days was minimal, while at 7 days, it is maximum. The maximum stiffness was achieved at 0.33 WTR with 90 days of curing. In general, the 90-day curing period provides a higher stiffness. At 0.36 WTR, the 28-day curing period has a lower stiffness when compared to 7-days. The mode-III stiffness values at 90-day are the highest for all three modes when comparing WTR.

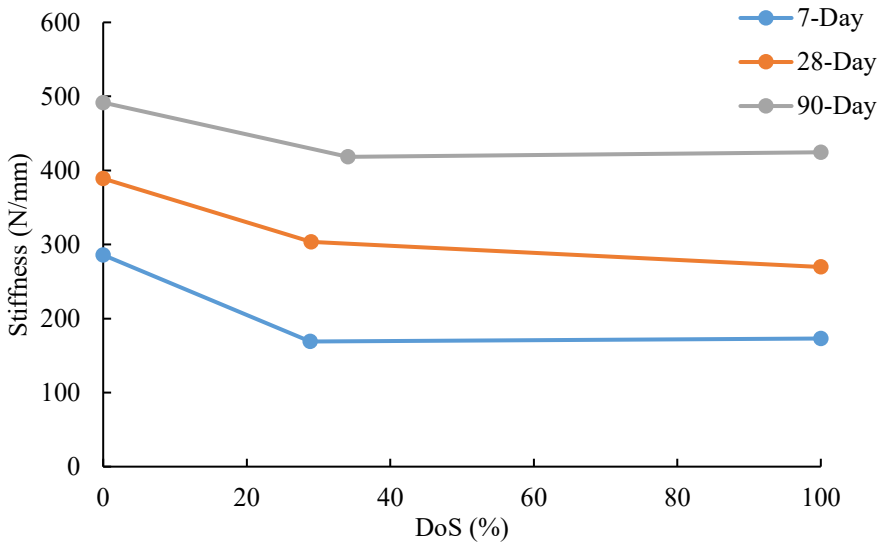

Figure 4.36: Effect of DoS on mode-III stiffness.

The stiffness observed in the samples follows a similar pattern to the work of crack initiation. In this graph, it is shown that the intermediate saturation is superior at 90 days. However, at the earlier stages of hydration, this intermediate saturation is weaker. The 7-day intermediate saturation point is higher than 28-days. Also, the 28-day sample in unsaturated conditions has a higher stiffness than 7-day or 90-day. At the fully saturated state, the 90-day curing period has the highest stiffness. The 90-day shows an increasing trend with an increase in DoS; the 28-day shows a decreasing trend.

4.2.4 Effect of hydraulic factor on fracture properties of CPB

When examining the porosity and saturation of these samples, it is noticeable how the increase in water content leads to increased porosity and an increase in the degree of saturation. The drained samples appear to have significant variance, and they may be more or less porous or saturated compared to the undrained samples. It could be that because the CPB is a pastelike material, the early drainage caused some loss of tailings or OPC binder. When compared to the 1B sample (Cc 0.045, WTR 0.36), it appears that the 1B sample has a higher porosity at the same curing times but a lower degree of saturation at seven days. At 28 days, the 1B saturation appears to fit between 2A and 2B, which is expected. In terms of fracture toughness, the Mode-II samples are again the weakest. It also shows that, depending on the loading, the samples can have a significantly different relation in terms of fracture toughness. For example, while the Mode-I 2E samples are much stronger than their equivalent 2D samples, in Mode-II, the 2D samples are stronger. Meanwhile, the 2C samples appear to do worse during the early ages but perform better at late ages. The most certain detail is that the WTR of 0.39 (Sample 2B) produced the weakest samples of the entire testing program. Another key note is that the effects of water content on the CPB fracture toughness is much less important compared to the effects of Cc. It is shown that when measuring the DoS and GWC, there are many cases where a WTR of 0.36 is optimum for the stiffness or work of crack initiation parameters. However, the overall effect of altering the water content proved to reap little benefit for the improvement of CPB. Using a WTR of 0.36 is the preferred choice for optimizing CPB fracture toughness while maintaining workability.

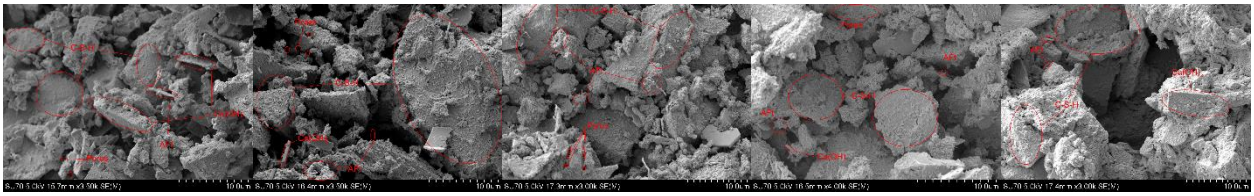

(A) 2A (B) 2B (C) 2C (D) 2D (E) 2E

Figure 4.37: Effect of water content on 7-Day microstructure of CPB.

Figure 4.37 shows the results of SEM for the hydraulic factor. In the 7-day SEM samples, the 2B sample with the highest initial water shows a wide variety of C-S-H sizes. While it has larger clusters that match the size of the 2A samples, it also has much smaller clusters similar to the 2C sample. Similar to the Cc samples, free AFt is more common in these samples than in the 90-day samples.

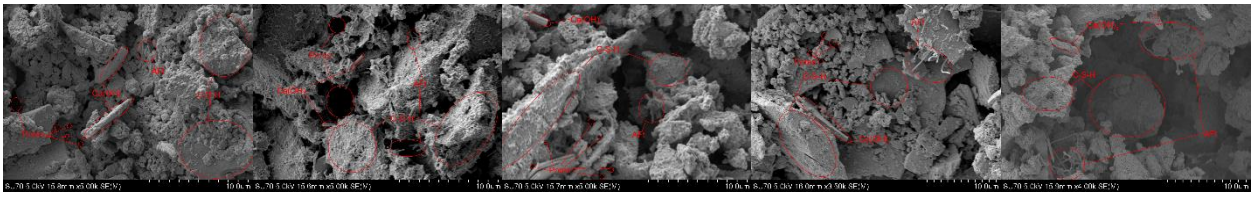

(A) 2A (B) 2B (C) 2C (D) 2D (E) 2E

Figure 4.38: Effect of water content on 28-Day microstructure of CPB.

Figure 4.38 shows the 28-day hydraulic factor samples, where there is an increase in the C-S-H cluster size when compared to 7-days. However, the difference is not very large. There are notable pore spaces in the 2B sample, which could be the result of the higher WTR for this sample. There are also smaller $Ca(OH)_2$ crystals in this sample. The drained sample has many smaller pores, which could be caused by the drainage as the water escapes from the sample. In the resaturated sample, there are some large C-S-H clusters, similar to the other samples. However, there are many small clusters, which could be caused by such resaturation process. The 2E sample shows a large void in the center of the image, with a lower layer of C-S-H.

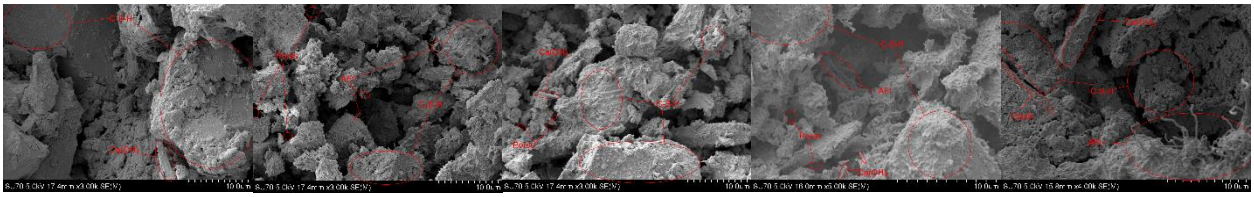

(A) 2A (B) 2B (C) 2C (D) 2D (E) 2E

Figure 4.39: Effect of water content on 90-Day microstructure of CPB.

Figure 4.38 shows the 90-day hydraulic factor sample's microstructure. In the 90-day samples, the amount of $Ca(OH)_2$ is very low. The 2A samples have the largest C-S-H clusters. The ettringite is most present in sample 2E. There is also a large gap in the center of the image. As with the previous samples, the relation between the different water conditions is consistent. However, there are much larger C-S-H clusters with smaller, uniform pores.

The microstructural analysis of these samples proves to reinforce the results of CPB improvement. Each sample shows a similar progression from 7-days to 90-days, and there is consistency between the different samples. For example, the lower WTR resulted in larger C-S-H particles, which corresponds to a better fracture toughness and higher stiffness.

Table 4.1: Effect of Water Drainage on Fracture Toughness.

	Mode 1			Mode 2			Mode 3		
	7	28	90	7	28	90	7	28	90
1B	9650.6	16954.0	28821.8	4095.5	5299.5	7890.9	5097.4	10263.5	12192.3
2C	12519.6	20344.8	29995.4	4202.9	7376.4	10592.6	5786.1	10745.7	15898.0

Table 4.2: Effect of Water Drainage on work of crack initiation.

	Mode 1			Mode 2			Mode 3		
	7	28	90	7	28	90	7	28	90
1B	2.1	4.9	19.9	14.4	12.2	50.0	85.6	177.2	171.3
2C	3.0	6.4	11.9	13.6	24.7	62.1	81.1	113.5	280.8

Table 4.3: Effect of Water Drainage on Stiffness.

	Mode 1			Mode 2			Mode 3		
	7	28	90	7	28	90	7	28	90
1B	140.6	178.4	284.0	183.2	242.1	325.2	169.0	219.8	418.4
2C	183.1	222.0	318.0	232.3	264.8	350.4	196.4	409.3	636.3

From the Table 4.1, it can be concluded that the drainage assisted in improving the fracture toughness. This effect is more pronounced in the 90-day samples. Table 4.2 shows that the effects are somewhat inconsistent in the work of crack initiation, as seen in the prior analysis with various samples. However, the majority of the results imply an increase in the required work as a result of the introduction of drainage. Finally, Table 4.3 shows that the stiffness is also improved with the added drainage effect. However, while it is an improvement, it appears the change due to reducing initial water content is more effective. By combining a reduced WTR and drainage, it is plausible that a more pronounced effect can be achieved.s

Chapter 5 Conclusions and recommendations

5.1 Conclusions

Several conclusions about the effects of cement hydration on CPB can be drawn from this discussion. First, the cement hydration affects both microscale and macroscale properties of CPB. In general, it was found that the CPB parameters improve with the hydration time. As hydration time is increased, it is found that the microstructure of CPB improves. Using Portland cement, when hydration time increases, the hydration products are generated and form a binding material that holds tailings together. This cement hydration continues as curing time increases, gradually improving the bond. This was confirmed using SEM to show the evolutive microstructure.

Microstructure and macrostructure properties are connected through the hydration process. What makes this clear is the correlation between the development of microstructure and the improvement of mechanical properties of CPB. These two are directly linked by the hydration time, curing stress, and curing temperature.

The increase in Cc is the most effective method of improving the CPB fracture toughness. While the reduction of the water content has proven to assist in the improvement of CPB, there is a limit to the effectiveness, especially at the 90-day and beyond. At an early age, the water content has a much more significant effect than the Cc. Drainage and saturation states, while having an effect, are relatively unimportant after 28 days of curing. For example, at 7 days of curing, a 7% Cc mix has a similar fracture toughness to a 2% Cc mix at 90 days. Meanwhile, even the best improvement due to water content adjustments results in slightly higher strength than a Cc of 4.5%.

Another clear conclusion is that the Mode-II loading condition is the main failure mode of CPB in fracture. This is due to the weak fracture toughness values obtained in Mode-II failure.

Looking at the Work of Crack Initiation, there is a trend of increased work required as the curing period increases. The Cc increase had a clear effect on the work, requiring the samples to do more work to achieve the crack initiation. However, when looking at the effect of hydraulic factors, the results are inconsistent depending on the curing age and mode examined. However, with only some exceptions, the higher curing period clearly required more work than the lower curing periods. Also, reducing the WTR led to higher work. The inconsistencies begin to appear when looking at the drained condition (2C) and the effect of the saturation state (2D, 2E).

The stiffness results fall into a similar problem as discussed in the work. However, in this case, there is an even less clear trend, even when examining the Cc effect. While there is a general trend of improvement with the increase in Cc, there are several exceptions, such as the mode-I 28-day sample. In general, the Mode-I samples have the lowest stiffness, while mode-II has the highest. This is in contrast to the fracture toughness results. However, the mode-III still has the intermediate values. The conclusion is that traditional stiffness measurements using fracture toughness testing are inaccurate. Therefore, it may be necessary to improve the accuracy.

With regards to the microstructural analysis, this method shows how the mixing process affected the properties of CPB and confirms that the effects of cement content and hydration are key to the CPB engineering properties. In particular, the fracture toughness is most improved by the increase in Cc. Meanwhile, changes in WTR or saturation state have a minimal effect. this can be observed by looking at the increased size of C-S-H clusters with the increasing Cc. Also, the curing age provides significant improvement to the microstructure of all CPB samples.

5.2 Recommendations for future work

The main recommendation of this work is that continued research into the fracture behavior of CPB is needed. For example, a better methodology for determining the stiffness of CPB would be beneficial for engineering design. In particular, the methodology used would not be sufficient for field-testing of CPB. This is due to the equipment required to prepare these samples for testing. In

addition, when reproducing this work, it is recommended to use computer numeric controlled (CNC) equipment to ensure the even cutting of the samples. By using this type of machine to prepare the samples, the width and depth of cuts can be precisely measured. This is mainly to ensure a higher precision result, which would be less likely to use manual cutting techniques. Using a CNC machine with proper vacuum dust collection could also reduce the exposure to dust. However, special care should be made to ensure no influence from additional materials, such as cooling fluid, is introduced. In addition, it would be of significant research interest if the samples were allowed to cure in water without significant damage to the sample. Another consideration is the use of alternative binder than OPC. Since the OPC is the main cost component, finding alternatives could lead to a significantly reduced cost of CPB. However, current studies which examine such (Carvalho et al, 2017, McLellan et al, 2011) do not consider the fracture behaviour. Therefore, re-examining the effectiveness of alternative binders with fracture condition should be examined.

References

Abell, A., Willis, K., Lange, D. 1999. Mercury Intrusion Porosimetry and Image Analysis of Cement-Based Materials, *Journal of Colloid and Interface Science*, 211:39â€“44

Araujo, E., Simon, D., Franca, F., Freitas Neto, O., and Santos Junior, O. 2016. Shear Strength of a Cemented Paste Backfill Submitted to High Confining Pressure, *Applied Mechanics and Materials*, 858: 219-224

Benmohamed, M., Alouani, R., Jmayai, A., Ben Haj Amara, A., Ben Rhaiem, H. 2016. Morphological Analysis of White Cement Clinker Minerals: Discussion on the Crystallization-Related Defects, *International Journal of Analytical Chemistry*, 2016

Benzaazoua, M., Fall, M., and Belem, T. 2003. A contribution to understanding the hardening process of cemented pastefill, *Minerals Engineering*, 17: 141-152

Benzaazoua, M.,Fall, M. Belem, T. A contribution to understanding the hardening process of cemented pastefill, *Minerals Engineering*, 141-152

Boháč, M., Kubátová, D., Nečas, R., Zezulová, A., Masárová, A., Novotný, R. 2016. Properties of Cement Pastes with Zeolite During Early Stage of Hydration, *Procedia Engineering*, 151:2-9

Carvalho, S. Z., Vernilli, F., Almeida, B., Oliveira, M. D., Silva, S. N. 2018. Reducing environmental impacts: The use of basic oxygen furnace slag in portland cement, *Journal of Cleaner Production*, 172:385-390

Chen, C., Li, X., Chen, X., Chai, J., Tian, H. 2019. Development of cemented paste backfill based on the addition of three mineral additions using the mixture design modeling approach, *Construction and Building Materials*, 229

Chen, s., Wu, A., Wang, Y., and Wang, W. 2020. Coupled effects of curing stress and curing temperature on mechanical and physical properties of cemented paste backfill, *Construction and Building Materials*, 273

Chen, S., Wu, A., Wang, Y., Wang, W. 2020. Coupled effects of curing stress and curing temperature on mechanical and physical properties of cemented paste backfill, *Construction and Building Materials*, 273

Cheng, H., Wu, S., Li, H. and Zhang, X. 2020. Influence of time and temperature on rheology and flow performance of cemented paste backfill, *Construction and Building Materials*, 231

Du, Z., Chen, S., Wang, S., Liu, R., Yao, D. And Mitri, H. 2021. Influence of Binder Types and Temperatures on the Mechanical Properties and Microstructure of Cemented Paste Backfill, *Advances in Civil Engineering*

Fall, M., Belem, T., Samb, S. and Benzaazoua, M. 2007. Experimental characterization of the stress-strain behavior of cemented paste backfill in compression, *Journal of Material Science*, 42:3914-3922

Fang, K. and Fall, M. 2018. Effects of curing temperature on shear behaviour of cemented paste backfill-rock interface, *International Journal of Rock Mechanics and Mining Sciences*, 112: 184-192

Jafari, M. 2020. Experimental Study of Physical and Mechanical Properties of a Cemented Mine Tailings, https://tspace.library.utoronto.ca/handle/1807/101293

Jafari, M. and Grabinsky, M. 2021. Effect of hydration on failure surface evolution of low sulfide content cemented paste backfill, *International Journal of Rock Mechanics and Mining Sciences*, 144

Komurlu, E., Kesimal, A., and Demir, S. 2016. Experimental and numerical analyses on determination of indirect (splitting) tensile strength of cemented paste backfill materials under different loading apparatus, Geomechanics and Engineering, 10 (6): 775-791

Li, L. 2015. Analytical solution for determining the required strength of a side-exposed mine backfill containing a plug, *Canadian Geotechnical Journal*, 51(5):508-519

Libos, I. and Cui, L. 2020. Effects of curing time, cement content, and saturation state on mode-I fracture toughness of cemented paste backfill, Engineering Fracture Mechanics, 235

Liu, L., Xin, J., Feng, Y., Zhang, B. and Song, K. 2019. Effect of the Cementâ€“Tailing Ratio on the Hydration Products and Microstructure Characteristics of Cemented Paste Backfill, *Arabian Journal for Science and Engineering*, 44: 6547â€“6556

Liu, L., Xin, J., Qi, C., Jia, H. and Song, K. 2020. Experimental investigation of mechanical, hydration, microstructure and electrical properties of cemented paste backfill, *Construction and Building Materials*, 263

Liu, L., Yang, P., Qi, C., Zhang, B., Guo, L., Song, KI I.I.L. 2019. An experimental study on the early-age hydration kinetics of cemented paste backfill, *Construction and Building Materials*, 212:283-294

Liu, L., Yang, P., Zhang, B., Huan, C., Lijie, G., Yang, Q. and Song, K. 2021. Study on hydration reaction and structure evolution of cemented paste backfill in early-age based on resistivity and hydration heat, *Construction and Building Materials*, 272

Liu, L., Zhua, C., Qi, C., Wang, M., Huan, C., Zhang, B., and Song, K. 2019. Effects of curing time and ice-to-water ratio on performance of cemented paste backfill containing ice slag, *Construction and Building Materials*, 228

McLellan, B., Williams, R., Lay, J., Van Riessen, A., Corder, G. 2011. Costs and carbon emissions for geopolymer pastes in comparison to ordinary portland cement, *Journal of Cleaner Production*, 19:1080-1090

Mozzaffaridana, M. 2011. Using Thermal Profiles of Cemented Paste Backfill to Predict Strength, *University of Toronto*

Oullet, S., Bussiere, B., Aubertin, M. and Benzaazoua, M. 2007. Microstructural evolution of cemented paste backfill: Mercury intrusion porosimetry test results, *Cement and Concrete Research*, 37: 1654-1665

Pan, A. and Grabinsky, M. 2021. Tensile Strength of Cemented Paste Backfill, *Geotechnical Testing Journal*, 44

Qi, C. and Fourie, A. 2019. Cemented paste backfill for mineral tailings management: Review and future perspectives, *Minerals Engineering*, 144

Sheshpari, M. 2015. A review on types of binder and hydration in cemented paste backfill (CPB), *Electronic Journal of Geotechnical Engineering*, 20:5949-5963.

Tariq, A. and Yanful, E. A review of binders used in cemented paste tailings for underground and surface disposal practices, *Journal of Environmental Management*, 131:138-149

Tian, X. and Fall, M. 2021. Non-isothermal evolution of mechanical properties, pore structure and self-desiccation of cemented paste backfill, *Construction and Building Materials*, 297

Wang, C., Ren, Z., Huo, Z., Zheng, Y., Tian, X., Zhang, K., Zhao, G. 2021. Properties and hydration characteristics of mine cemented paste backfill material containing secondary smelting water-granulated nickel slag, *Alexandria Engineering Journal*, 60: 4961-4971

Weilv, W., Xu, W., Jianpin, Z. 2021. Effect of inclined interface angle on shear strength and deformation response of cemented paste backfill-rock under triaxial compression, *Construction and Building Materials*, 279

Xiu, Z., Wang, S., Ji, Y., Wang, F., Ren, F., Nguyen, V. 2021. The effects of dry and wet rock surfaces on shear behavior of the interface between rock and cemented paste backfill*, Powder Technology*, 381:324-327

Xu, W., Tian, X. and Cao, P. 2017. Assessment of hydration process and mechanical properties of cemented paste backfill by electrical resistivity measurement, *Nondestructive Testing and Evaluation*, 32

Xu,W., Li, Q. and Liu, B. 2020. Coupled effect of curing temperature and age on compressive behavior, microstructure and ultrasonic properties of cemented tailings backfill, *Construction and Building Materials*, 237

Zhang, B., Xin, J., Liu, L., Lijie, G. and Song, K. 2018. An Experimental Study on the *Microstructures of Cemented Paste Backfill during Its Developing Process*, Advances in Civil Engineering

Zhou, X., Hu, S., Zhang, G., Li, J., Xuan, D., Gao, W. 2019. Experimental investigation and mathematical strength model study on the mechanical properties of cemented paste backfill, *Construction and Building Materials*, 226:524-533